Published in final edited form as:

J Immunol. 2021 September 01; 207(5): 1357–1370. doi:10.4049/jimmunol.2001395.

Critical Role of Zinc Transporter (Zip8) in Myeloid Innate Immune Cell Function and the Host Response against Bacterial Pneumonia

Sannette C. Hall[*], **Deandra R. Smith**[*], **Shetty Ravi Dyavar**[*], **Todd A. Wyatt**[†,‡,§], **Derrick R. Samuelson**[‡], **Kristina L. Bailey**[‡,§], **Daren L. Knoell**[*]

[*]College of Pharmacy, Department of Pharmacy Practice and Science, University of Nebraska Medical Center, Omaha, NE 68198-6120

[†]College of Public Health, Department of Environmental, Agricultural and Occupational Health, University of Nebraska Medical Center, Omaha, NE 68198-6120

[‡]College of Medicine, Department of Internal Medicine-Pulmonary Division, University of Nebraska Medical Center, Omaha, NE 68198-6120

[§]Department of Veterans Affairs Nebraska-Western Iowa Health Care System, University of Nebraska Medical Center, Omaha, NE 68198-6120

Abstract

Zinc (Zn) is required for proper immune function and host defense. Zn homeostasis is tightly regulated by Zn transporters that coordinate biological processes through Zn mobilization. Zn deficiency is associated with increased susceptibility to bacterial infections including *Streptococcus pneumoniae*, the most commonly identified cause of community acquired pneumonia. Myeloid cells, including macrophages and dendritic cells (DCs), are at the front line of host defense against invading bacterial pathogens in the lung and play a critical role early on in shaping the immune response. Expression of the Zn transporter ZIP8 is rapidly induced following bacterial infection and regulates myeloid cell function in a Zn-dependent manner. To what extent ZIP8 is instrumental in myeloid cell function requires further study. Using a novel myeloid-specific, *Zip8* knockout (KO) model, we identified vital roles of ZIP8 in macrophage and DC function upon pneumococcal infection. Administration of *S. pneumoniae* into the lung resulted in increased inflammation, morbidity and mortality in *Zip8*-KO mice compared to wild type (WT) counterparts. This was associated with increased numbers of myeloid cells, cytokine production, and cell death. *In vitro* analysis of macrophage and DC function revealed deficits in phagocytosis and increased cytokine production upon bacterial stimulation that was, in part, due to increased NFκB signaling. Strikingly, alteration of myeloid cell function resulted in an imbalance of Th17/Th2 responses, that is potentially detrimental to host defense. These results for the first time reveal a vital ZIP8- and Zn-mediated axis that alters the lung myeloid cell landscape and the host response against pneumococcus.

Corresponding Author Phone Number: 402-559-9016, Fax Number: 402.559.5673, daren.knoell@unmc.edu.

Introduction

Community acquired pneumonia (CAP) is a leading cause of morbidity and mortality worldwide. *Streptococcus pneumoniae* (pneumococcus) is the most prevalent pathogen causing CAP in the U.S. resulting in increased hospitalizations and mortality (1-4). A major predisposing factor for the increased incidence of CAP is a decline in immune function in vulnerable populations (5). Daily dietary Zn intake is required for human health and proper immune function. Despite this, nutritional deficiency remains prevalent within vulnerable populations (6-9). In fact, ~17% of the world's population is at risk of inadequate zinc intake (10). Dietary Zn deficiency increases susceptibility to pathogens (11) and is associated with a higher incidence of pneumonia (12, 13) while Zn supplementation has been shown to reduce risk (14-16).

The mechanisms by which Zn bolsters immune function and protects against pathogen invasion remain to be fully elucidated. Zn homeostasis in mammals is tightly regulated by two major Zn transporter/carrier families known as Solute Carrier Family (SLC) 30 and 39. The SLC39 or *a.k.a* ZIP (Zrt-, Irt-like proteins) family is comprised of 14 members that primarily function to increase cytosolic Zn concentrations. Through Zn mobilization, ZIPs help regulate the function of enzymes, receptors and transcription factors as well as cytokine and growth factor-mediated signaling pathways (17, 18). Our group was the first to reveal that the Zn transporter ZIP8 is unique relative to other family members in that it is required by myeloid-lineage cells to balance host defense and the inflammatory response against bacteria (19-21). More recently, human studies have revealed that a frequently occurring ZIP8 variant allele that leads to defective intracellular transport (rs13107325; Ala391Thr risk allele) is strongly associated with inflammation-based disorders (22, 23) and bacterial infection (24). In fact, the SLC39A8 (rs13107325) polymorphism is one of the most pleiotropic variants in the human genome, ranking 9th of 341 genomic regions associated with more than one human disease or trait in genome wide association studies (GWAS) (23).

Myeloid innate immune cells, namely macrophages and dendritic cells, form the front-line defense against invading pathogens in the lungs. Both cell types express multiple pattern recognition receptors (PRRs) that allow for the detection of unwanted invaders and subsequent orchestration of the immune response (25). Despite the close physical proximity and functional relationships that exist between macrophages and DCs (25, 26), they are rarely examined together in the context of infectious disease.

Alveolar macrophages (AMs) are the primary resident phagocytes in the lung. They are ideal sentinels based on their location, phagocytic capacity, and expression of PRRs. Alveolar macrophages employ a range of strategies to phagocytose and kill pathogens. When the capacity to clear pathogens is overwhelmed, macrophages play an important role in orchestrating the inflammatory response by secreting multiple cytokines and chemokines that recruit and activate other immune cells (25, 26). AMs have been shown to play critical roles in host defense against *S. pneumoniae* mediating the initiation and termination of inflammation, as well as subsequent restoration of lung homeostasis (27-30).

Dendritic cells are professional antigen presenting cells that bridge the gap for communication between innate and adaptive immunity. Lung DCs reside in an immature state, but with the ability to quickly recognize and capture invading pathogens. Upon pathogen recognition, DCs mature, produce multiple inflammatory factors, and ultimately migrate to the draining lymph nodes where they present processed antigens to T-cells, thereby inducing antigen-specific immune responses (31, 32). A role for DCs in the pathogenesis of pneumococcal lung infection is only just emerging. Recent studies have shown that imbalance leading to excessive DC function facilitates extrapulmonary migration of *S. pneumoniae* leading to increased inflammation, bacterial dissemination, and mortality (33, 34).

Although Zn homeostasis has an established role in mediating cellular activation against pathogens, more investigation is warranted to determine the essentiality of Zn and ZIP8 in myeloid cell function in the lung. Taken together, we hypothesized that ZIP8 plays a vital role in myeloid cell mediated responses, especially in macrophages and DCs, and that loss of ZIP8 function will adversely impact the host response to pneumococcus through altered myeloid cell function. Using a novel myeloid-specific *Zip8*-KO mouse model, we observed significant increases in cytokine production, inflammation and mortality in *Zip8*-KO mice following pneumococcal infection. This was associated with increased lung myeloid cell infiltration and bacterial dissemination. Further *in vitro* analyses of macrophage and DC function revealed impaired phagocytosis and increased cytokine production upon bacterial stimulation, which was found to be, in part, due to increased NFκB signaling. Loss of *Zip8* expression also led to profound alterations in T-cell programming which we postulate is further detrimental to host defense. These results for the first time reveal a vital axis that involves Zn homoeostasis, myeloid cell function, and the host response against pneumococcus in the lung and reveals a molecular pathway that is accountable for the defects observed in host defense. Further study is warranted to determine whether novel micronutrient surveillance and treatment strategies can improve our ability to prevent or treat pneumococcal pneumonia.

Materials and Methods

Animals and Care

All animals were maintained under specific pathogen-free conditions in the Animal Resource Facility at the University of Nebraska Medical Center. Food and water were provided *ad libitum*. The research protocol used in these studies was approved by the Institutional Animal Care and Use Committee of the University of Nebraska Medical Center. All methods involving animal care and procedures in this research protocol were performed in accordance with the NIH and Office of Laboratory Animal Welfare (OLAW) guidelines.

Conditional *Zip8* knockout mice; herein referred to as *Zip8*-KO, were generated as previously described (35). Briefly, heterozygous $Zip8^{\text{flox-neo/+}}$ mice were bred to ROSA26:FLPe knock-in mice (The Jackson Laboratory, Bay Harbor, ME) with ubiquitous expression of FLP1 recombinase to delete the Neo cassette adjacent to the upstream loxP site. The resulting $Zip8^{\text{flox/+}}$ were mated to produce $Zip8^{\text{flox/flox}}$ mice. PCR and DNA sequencing confirmed removal of the FRT-flanked sequence and verified the loxP sites

flanking exon 3. *Zip8*$^{flox/flox}$ mice were crossed to myeloid cell specific LysMcre (The Jackson Laboratory) to generate the conditional *Zip8*-KO. LysMcre mediated Zip8 deletion was confirmed in lung myeloid cells at baseline and 24-hours post LPS stimulation using a ROSA reporter (supplemental figure 1). C57BL/6J wild-type counterparts were purchased from Jackson Labs and bred for experimental procedures.

Culture, Quantification, and Instillation of Streptococcus pneumoniae

S. pneumoniae strain JWV500 (D39hlpA-gfp-Cam'), a generous gift from Dr. Jan-Willem Veening (University of Lausanne, Switzerland), were grown to mid-log phase, aliquoted, frozen and stored at −80 °C until further use. For lung infection studies, bacteria were grown to log phase in Remel Mueller Hinton Broth (Fisher Scientific, Lenexa, KS) supplemented with 32 mg/ml chloramphenicol. For quantification of pneumococci, serial dilutions of the bacteria were plated on Remel blood agar plates (Fisher Scientific), incubated at 37 °C with 5% CO_2 overnight to determine colony forming units (CFUs). For intranasal instillations, mice were lightly anesthetized using 2% isoflurane and 1 L/min of oxygen and instilled with 4 x 10^8 CFU of *S. pneumoniae* in 100 μl of phosphate buffered saline (PBS) equally distributed (2 x 50 μl) between the nostrils. Mice were allowed to recover between nasal instillation doses to prevent respiratory distress. *S. pneumoniae* dose was confirmed by serial dilutions.

Bronchoalveolar Lavage Fluid (BALF) Analyses

Lungs were lavaged three times with 1 ml ice-cold PBS. Total cell counts were determined using a hemocytometer and differential cell counts were determined on cytospin prepared slides stained with Hema-3 (Fisher Scientific, Pittsburg, PA). Cytokine and chemokine levels were measured using commercially available ELISA kits according to manufacturers' instructions (BioLegend, R&D Systems).

Lung Histology

Whole lungs were inflated with 10% formalin (Fisher Scientific) to preserve pulmonary architecture. Lungs were processed, paraffin embedded, sectioned (4-5 μm) and stained with hematoxylin and eosin by the UNMC Tissue Sciences Core Facility. Slides were scanned using the Ventana HT iScan (Roche Diagnostic, Mannheim Germany) and images acquired (20 x) using the Ventana Image Viewer software (Roche). Slides were reviewed and semi-quantitatively assessed (assigned a score from 0 to 5, with a higher score indicting greater inflammatory changes) by a veterinary pathologist blinded to treatment conditions.

Tissue Immunostaining

TUNEL Staining—Formalin fixed paraffin embedded (FFPE) lung sections were stained for in situ apoptosis detection using the Click-IT Plus TUNEL Assay Alexa 594 (ThermoFisher) according to manufacturer instructions. Images were visualized using a Zeiss Observer Z1 inverted phase contrast fluorescent microscope (Carl Zeiss Microscopy, LLC, White Plains, NY) and Alexa 594 fluorescent intensity was quantified using the Image J software (NIH).

Caspase-3 Staining—FFPE lung sections were stained for caspase-3 expression by the UNMC Tissue Sciences Core Facility using standardized protocols. Briefly, slides were stained with caspase-3 primary antibody (Abcam, Cambridge, MA), washed, incubated with anti-HRP antibody, washed, stained with H_2O_2 and DAB ChromoMap (Roche), and counterstained with hematoxylin. Slides were scanned using the Ventana HT iScan (Roche) and images acquired (40 x) using the Ventana Image Viewer software (Roche).

Tissue Processing

Lung lobes were collected and perfused with digestion solution containing 1x HBSS (Hyclone, GE Healthcare Lifesciences, Logan, UT), 1 mg/ml collagenase D (Roche), and 20 μg/ml DNase (Roche), incubated for 30 minutes at 37 °C, and homogenized using gentleMACS™ Octo Dissociator (Miltenyi Biotec, Auburn, CA). After enzymatic digestion and red blood cell lysis (1x RBC Lysis Buffer, Invitrogen by Thermo Fisher Scientific, Life Tech Corp, Carlsbad, CA), samples were resuspended in FACS rinsing buffer (1 x PBS supplemented with 4% FBS and 20% sodium azide) for cell surface staining.

Isolation and Generation of Bone Marrow-Derived Macrophages (BMDMs) and Dendritic Cells (BMDCs)

BMDMs—BMDMs were generated from WT and *Zip8*-KO mice (7-10 weeks old) as previously described (36). Briefly, femurs and tibias were harvested from mice in both groups, and bone marrow cells plated in DMEM containing 2mM glutamine and supplemented with 10% FBS, Pen/Strep (Gibco) and 20% L929 conditioned medium, as a source of M-CSF. Cells were plated at a density of 5 x 10^5 cells/ml in 100 mm dishes. Cells were grown for 3 days, and fresh media supplemented with 20% L929 conditioned medium was added on day 3. Cells were incubated for an additional 4 days prior to further experimentation.

BMDCs—Bone marrow-derived dendritic cells (BMDCs) were generated as previously described (37) with a few modifications. Briefly, the femurs and tibias from C57BL/6 WT and *Zip8*-KO mice (7-10 weeks old) were harvested, and bone marrow cells were plated in RPMI-1640 (Hyclone) supplemented with 10% FBS, Pen/Strep (Gibco) and 50 μM β-mercaptoethanol (MP Biomedical, Solon, OH) at a density of 1 x 10^6 cells/ml in 6 well plates. The cell culture media was supplemented with 20 ng/ml recombinant mouse granulocyte monocyte-colony stimulating factor (GM-CSF) and 20 ng/ml interleukin (IL) - 4 (PeproTech, Rocky Hill, NJ). Fresh media supplemented with GM-CSF and IL-4 (3 ml per well) was added to the plates on days 3 and 6. On day 8, the non-adherent and loosely adherent fraction was collected for CD11c isolation. Immature BMDCs (day 8) were harvested from cell culture plates, centrifuged at 250 *x g* for 10 minutes, resuspended in MACS buffer and incubated with CD11c ultrapure magnetic beads (Miltenyi Biotec) according to the manufacturer's protocol. The $CD11c^+$ fraction was isolated, and cells resuspended in DC media (RPMI supplemented with IL-4 and GM-CSF) for subsequent studies.

BMDM Phagocytosis Assay

Bacteria were prepared as previously described and labelled with 5 μM CFSE at 37 °C for 30 minutes. Following CFSE labelling, bacteria were washed and incubated with WT and *Zip8*-KO BMDMs plated at a density of 5 x 10^5 cells/ml on 12-well plates (MOI=10). Plates were centrifuged at 200 x g for 5 minutes and incubated for 1 hour to allow for bacteria internalization. Cells were then washed three times with ice cold PBS to remove unbound bacteria, harvested and stained with cell surface markers for flow cytometry. For detection of background fluorescence, BMDMs from both groups were incubated with *S. pneumoniae* at 4 °C. Median fluorescent intensity (MFI) of CFSE was used as a measure of phagocytosis after subtracting MFI of the 4 °C *S. pneumoniae* sample from the 37 °C *S. pneumoniae* sample ($MFI\ CFSE_{sample} = MFI\ CFSE_{sample\ @37\ °C} - MFI\ CFSE_{sample\ @4°C}$). To ensure viability of bacteria after CFSE labelling, aliquots were serially diluted and plated on blood agar plates to determine CFUs.

BMDC Activation

BMDCs were plated at a density of 5 x 10^5 cells/ml on to 12-well plates and incubated with either 1 μg/ml lipopolysaccharide (LPS) from *E. coli* (Cat. # L4516; MilliporeSigma, St. Louis, MO) or 10 μg/ml lipoteichoic acid (LTA) from *Staphylococcus aureus* (Cat. # L2515; MilliporeSigma) for 6 hours. Cells and supernatants were harvested for downstream analyses.

Fluorescence activated cell sorting (FACS)

BMDCs and/or whole lung lysates were incubated with Zombie UV Fixable Viability Kit (BioLegend, San Diego, CA) at room temperature for 15 minutes. Cells were washed with FACS rinsing buffer, pelleted, and incubated with anti-mouse CD16/32 (BioLegend) for 15 minutes at 4 °C to block non-specific Ig binding. Following subsequent washing and centrifugation, cells were incubated with antibody cocktails containing some or all of the following markers: CD11c BV711, CD80 BV650, CD64 PerCP/Cy5.5, Ly6C BV605, CCR-7 APC, MHC-II (I-A/I-E) BV 421, Ly6G BV650, CD40 PE/Cy7,CD4 APC/Cy7, CD3 APC, and CD8α PerCP/Cy5.5 (BioLegend); CD86 BUV395, CD11b BV480, Siglec-F APC-R700, CD45 BV805, CD103 PE-CF594, and CD24 BUV 737 (BD Biosciences, San Jose, CA). Cells were analyzed using the BD LSRFortessa™ (BD Biosciences). Cell aggregates were removed by gating single cells on the forward light scatter (FSC-H vs FSC-A). Dead cell and debris were excluded before gating for myeloid innate immune cells and/or T-cell markers. Fluorescence minus one (FMO) controls were used to set up gating strategies used in these experiments. Data was analyzed using FlowJo software v10.7.1 (Tree Star Inc.).

RNA Isolation and Gene Expression Analysis

Total RNA was isolated from BMDCs using the RNeasy Mini Kit (Qiagen, Hilden, Germany) per manufacturer's instructions and total RNA yield quantified using Nanodrop One (Thermo Fisher Scientific, Waltham, MA). The isolated RNA was then reverse transcribed using the High Capacity cDNA Transcription Kit (Applied Biosystems, Thermo Fisher Scientific). Quantitative real-time PCR was performed

using the 7500 Real-Time PCR System (Applied Biosystems). Forward and reverse primers used were as followed: *Zip6* 5'- ACAACGCTGTCTCTGAAGGA-3' and 5'-AAGCTCTTTCTGGGCTCACT-3'; *Zip8* 5'-CAGTTGCTGTGTTTGGTGGA-3' and 5'-GCATAGCAAGTCACACCGTT-3'; *Zip10* 5'-TGTTGAAAGGACTTGTGGCG-3' and 5'-TACCGAGTCATCCGTTCCAG-3'; and *Zip14* 5'-GGAAGATCTCATGGACCGCT-3'and 5'-AGAATGGTGGGGCAGAACTC-3' (Integrated DNA Technologies, Coralville, IA). Relative gene expression was normalized against the housekeeping gene, glyceraldehyde-3-phosphate dehydrogenase (GAPDH) and fold-change in mRNA expression determined using $^{\Delta\Delta}$Ct method (38).

Gene expression profiling was performed using the NanoString nCounter system (NanoString Technologies, Seattle, WA). Specifically, mouse myeloid cell innate immune response genes were profiled using the nCounter® Mouse Myeloid Innate Immunity Panel v2 according to the manufacturer's instructions. Briefly, 50 ng of total RNA per sample was hybridized overnight and loaded on to a cartridge via the nCounter MAX/FLEX System, set to the high sensitivity setting. The cartridge was stored overnight, in the dark, at 4°C before loading onto the nCounter Digital Analyzer. Gene expression was normalized against 20 internal reference genes and data analysis was performed using nSolver™ 4.0 Analysis Software (NanoString Technologies).

Ingenuity Pathway Analysis (IPA) software (Qiagen) was used to perform pathway enrichment, gene network, and upstream regulator analyses according to the standard protocols as previously described (39, 40). A list of differentially expressed genes in a dataset with a minimum of 1.5-fold change and p value of < 0.05 significance were compared between the two groups and uploaded into IPA. Core analysis was performed on uploaded datasets based on fold change and p value significance to determine the biological pathways significantly (< 0.05 p value and , > 0.05 ratio of differentially regulated genes involved in a pathway with the number of genes associated with the pathway) regulated in a dataset according to a standard protocol as previously described (41). A gene transcriptional network analysis was performed to identify transcripts that were significantly regulated, and part of a transcriptional network destined to perform a specific biological function. This, in turn, was used to mechanistically identify key or central regulators of a transcriptional network. Upstream regulator analysis was performed to identify secretory factors, signaling mediators and transcription factors that may not have been differentially expressed at the transcription level but are predicted to be post-translationally altered or modified (phosphorylation, acetylation, and methylation) at the protein level with significant (< 0.05 p value and $> \pm 2.0$ Z score) activation or inhibition.

Western Blotting

Cell lysates were obtained using standard cell lysis buffer (Cell Signaling, Danvers, MA) containing 1mM phenylmethylsulfonyl fluoride (PMSF). Proteins were separated by SDS-PAGE and transferred to nitrocellulose membranes (Thermo Fisher). The membranes were blocked with 5% BSA (Sigma-Aldrich) in TBS, followed by probing for antibodies overnight. All primary antibodies were purchased from Cell Signaling Technology, Inc.

Protein detection and analysis was done using the Odyssey Image System (Li-Cor, Lincoln, NE).

Inhibition Studies

BMDCs were primed with 10 μM Bay 11-7082 (MilliporeSigma) or vehicle control for 1 hour. Cells were washed 3 times with media then stimulated with 1 μg/ml LPS for designated time points. Whole cell lysates were obtained with standard cell lysis buffer (Cell Signaling) containing 1 mM PMSF. Protein concentrations were obtained using the Pierce BCA protein assay (Thermo Fisher).

NFκB Translocation (Flow Cytometry)

WT and *Zip8*-KO BMDCs were primed with the inhibitor as described above, washed, and stimulated with LPS (1 μg/ml) for 15 minutes. Cells were harvested, washed, fixed and permeabilized in 150 μl of Cyto-Fast™ Fix/Perm buffer (BioLegend) for 20 minutes. Following fixation, cells were washed with 1 ml Cyto-Fast™ Perm Wash solution, centrifuged (250 x g for 10 minutes) and re-suspended in Cyto-Fast™ Perm Wash solution for staining. Fixed and permeabilized cells were stained with NFκB p65 FITC (Santa Cruz Biotechnology, Dallas, TX) for 20 minutes at room temperature, washed, stained with DRAQ5™ (Immuno Chemistry Technologies, Bloomington, MN) and analyzed using Amnis® FlowSight® Imaging Flow Cytometer (Luminex, Austin,TX).

Zinc Quantification

Zn was semi-quantified at baseline and in stimulated (LPS or LTA, 6 hours) WT and *Zip8*-KO BMDCs by incubating cells with 1 μM Zinpyr-1 (MilliporeSigma) for 30 minutes. Following incubation, cells were washed three times and harvested for cell surface staining (for DC markers). ZinPyr-1 fluorescent intensity was measured by FACS, and Zn levels quantified as median fluorescent intensity (MFI) of ZinPyr-1.

Zinc Chelation and Supplementation

BMDCs from WT and *Zip8*-KO mice were incubated with either 1 μM tris 2-pyridylmethyl amine (TPA) or 0.1 μM Zn sulfate ($ZnSO_4$) for 30 minutes in Zn free RPMI. Cells were washed twice with RPMI and stimulated with 100 ng/ml of LPS for 24 hours. Supernatants were collected for cytokine expression.

$CD4^+$ T-cell responses in vivo and ex vivo

WT and *Zip8*-KO mice were infected with *S. pneumoniae* as previously described and mediastinal lymph nodes harvested 72 hours post infection. Lymph nodes were processed into single cell suspensions, stained with an antibody cocktail consisting of CD11c, MHC-II, CD24, CD64, CD80, CD86, CD40, CD45, CD3, CD8α and CD4 (BD Biosciences and BioLegend) and DC and T-cell populations were then phenotyped by flow cytometry.

To characterize $CD4^+$ T-helper cell subsets, lymph node cell homogenates from WT and *Zip8*-KO infected mice were stimulated *in vitro* with a cell activation cocktail containing PMA (10 ng/ml; StemCell Technologies, Vancouver, Canada), ionomycin (250 ng/ml; StemCell Technologies) and Brefeldin A (5 μg/ml; BioLegend) for 4 hours. Cells

were harvested, washed, stained for surface markers as previously described, fixed and permeabilized for 20 minutes with CytoFastFix/Perm (BioLegend), washed and then stained with an antibody cocktail containing IL-2 APC, IL-4 PE/Dazzle594, IFN-γ PE and IL-17 BV421 (BioLegend). Intracellular cytokine production of the $CD4^+$ T-cell subset was characterized by flow cytometry.

For cytokine detection by ELISAs, LN leukocytes were stimulated with PMA (10 ng/ml) and ionomycin (250 ng/ml) for 48 hours. Supernatants were collected for measurement of IL-2, IFN-γ, IL-4 and IL-17A/F according to manufacturers' instructions.

ELISA

Cytokine levels (TNF-α, IL-2, IL-4, IL-17A/F, IL-6, IL-10, IL-12/23p40, IFN-γ and CXCL-1) were determined using commercially available ELISA kits (BioLegend and R&D, Minneapolis, Mn) according to manufacturer's instructions. Assay sensitivities were: IL-6 and CXCL-1 (2 pg/ml), TNF-α, IFN-γ and IL-12/23p40 (4 pg/ml), IL-10 (16 pg/ml), IL-17A/F (2.3 pg/ml), IL-2 and IL-4 (1 pg/ml).

Statistical Analyses

Data were analyzed using GraphPad Prism version 8.00 (GraphPad Software, La Jolla, CA). Unpaired Student's t-test was used to determine differences between groups. Multiple group comparisons were made using ANOVA with Tukey's post-hoc tests. Values are expressed as means ± SEM. A value of $p \leq 0.05$ was considered significant.

Results

Loss of Zip8 is associated with increased lung injury and mortality following S. pneumoniae infection.

To determine the role of ZIP8 in the immune response following pneumococcal infection, WT and *Zip8*-KO mice were administered via intranasal installation a dose of 4×10^8 CFU *S. pneumoniae* and monitored over a 7-day period. *Zip8*-KO mice were observed to have increased morbidity and mortality following pneumococcal infection in the lung (Figure 1). By the end of the fourth day post instillation, approximately 40% of the *Zip8*-KO mice had succumbed to the infection compared to only 5% in the WT group ($p < 0.01$; Figure 1A). Based on this observation, we next examined the immune response at 72 hours post infection. Mice were administered 4×10^8 CFU *S. pneumoniae* and tissues were harvested for further analysis. Histological staining of lung tissue revealed that *Zip8*-KO mice had increased lung injury, as determined by inflammatory score, and increased cell death, as determined by TUNEL and caspase-3 staining (Figure 1B-E). This response persisted in the surviving *Zip8*-KO mice up to 7 days post infection as observed by histological and BAL fluid analysis of lung tissue from survivors (Supplemental Figure 2A-D).

Zip8-KO increases cellular infiltration and lung inflammation within 24 hours and up to 72 hours following bacterial instillation.

To examine the early immune response against *S. pneumoniae* in the lung, WT and *Zip8*-KO mice were administered 4×10^8 CFU *S. pneumoniae* and euthanized 24 or 72 hours later.

Analysis of BAL fluid from the lungs revealed that bacterial instillation resulted in increased total numbers of leukocytes in the airways of both groups when compared to the uninfected mice at 24 and 72 hours post infection. Macrophages and neutrophils were the main subsets of leukocytes identified. The *Zip8*-KO mice exhibited higher numbers of macrophages at 24 hours post infection which persisted up to72 hours post infection (Figure 2A) and higher numbers of neutrophils 24 hours post infection (Figure 2B). Pneumococcal infection was also associated with increased expression of IL-6, TNF-α and IL-12/23 (p40 subunit) in both groups, with IL-12/23p40 trending higher in the *Zip8*-KO group when compared to WT animals ($p = 0.055$; Figure 2C-E). Taken together, these results demonstrate an imbalance in the cellular landscape and immune response to *S. pneumoniae* as a consequence of ZIP8 loss.

Zip8 loss alters lung cellularity in a manner that promotes tissue injury and mortality.

Knowing that macrophages and DCs play critical roles in orchestrating the immune response after bacterial infection, and that we observed increased mortality between 72 to 96 hours post infection, we next characterized the lung tissue population of both cell types, including DC subsets, at 72 hours post infection. Mice were infected with *S. pneumoniae* (4×10^8 CFUs) and tissues were harvested for further analyses. Immune cells in lung homogenates from both groups were characterized using flow cytometry. After gating out debris and doublets, live $CD45^+$ leukocytes were selected. Cells were characterized as AMs, based on expression of CD11c, Siglec F and CD64 ($CD45^+CD11c^+$Siglec F^+ $CD64^+$), or DCs, based on expression of classic DC markers ($CD45^+CD24^+CD64^-CD11c^+MHC\text{-}II^+$; Supplemental Figure 1). DC subsets were then identified based on expression of CD11b or CD103. There was an increase in total macrophage and DC numbers in both groups from 24 to 72 hours post infection. At 72 hours post infection, the *Zip8*-KO group exhibited increased DC numbers compared to WT animals (Figure 3A-B). Further analysis of DC subsets revealed an increase in the total numbers of $CD11b^+$ DCs in the lungs of *Zip8*-KO mice (Figure 3C), that consisted of a mix of resident/conventional DCs ($CD11b^+Ly6c^-$) and overall greater numbers of inflammatory monocyte derived DCs ($CD11b^+Ly6c^+$) when compared to the WT counterparts (data not shown). These results further demonstrate that Zip8 loss aggravates the inflammatory response at least in part through alteration of the lung macrophage and DC landscape in response to pneumococcal infection.

Loss of Zip8 is associated with impaired macrophage phagocytosis and increased bacterial dissemination.

To determine whether increased lung APC presence and increased lung tissue damage altered bacterial dissemination, bacterial counts were enumerated from the spleens of both groups. *Zip8*-KO mice had significantly higher bacterial burden in spleens 72 hours post infection (Figure 4A). Given that increased numbers of macrophages were associated with increased bacterial dissemination in *Zip8*-KO mice, we questioned whether macrophage phagocytosis was impaired by ZIP8 loss. To further examine the impact of ZIP8 loss on phagocytosis, BMDMs were generated from WT and *Zip8*-KO mice, incubated with CFSE labelled *S. pneumoniae* for 1 hour, and bacterial uptake determined by flow cytometry. Cells were gated based on expression of cell surface markers ($CD11b^+CD24^-CD64^+$), with > 90% of the population phenotyped as macrophages (data not shown). Further analysis of the gated

cells revealed that BMDMs generated from *Zip8*-KO mice had impaired bacterial uptake as measured by the median fluorescent intensity of CFSE, after subtracting the MFI of the control sample (4 °C) from that of the test sample (37 °C; Figure 4B-C). Similar results were observed with *E. coli* (pHrodo *E. coli*; ThermoFisher) up to 2 hours post incubation (data not shown). These results demonstrate that ZIP8 loss significantly alters the phagocytic capacity of macrophages which may contribute to increased bacterial dissemination as observed in *Zip8*-KO animals post pneumococcal infection.

Phenotypic characterization and cytokine production of BMDCs after bacterial stimulation

Given the increase in DCs and inflammatory cytokines observed in the lungs of *Zip8*-KO mice from 24 to 72 hours post infection, the next step was to determine whether ZIP8, or lack thereof, has direct impact on DC function as well. To examine the impact of ZIP8 loss upon DC function, BMDCs were generated from WT and *Zip8*-KO mice and then stimulated with gram-negative and gram-positive bacterial cell wall extracts. LPS and LTA stimulation induced a similar pattern of BMDC maturation in both groups compared to unstimulated cells. In particular, DC maturation was associated with increased expression of MHC-II, CD80/86, CD40 and CCR-7 in LPS- and LTA-pulsed WT and *Zip8*-KO BMDCs (data not shown).

Although there were no significant differences observed in maturation markers expressed by stimulated DCs from both groups, there were stark differences in the cytokine response to LPS and LTA stimulation (Figure 5A-D). *Zip8*-KO stimulated BMDCs had significantly higher production of IL-12/23 p40 (LPS – $p < 0.01$; LTA – $p < 0.05$), IL-6 (LPS and LTA, $p < 0.01$), and TNF-α (LTA only, $p < 0.001$). In contrast, WT BMDCs produced more IL-10 (LPS – $p < 0.001$; LTA – $p < 0.05$) compared to *Zip8*-KO cultures following stimulation. There were no differences observed in the production of CXCL-1 between the groups (Figure 5E). Collectively, the data demonstrate that ZIP8 loss does not alter DC maturation in response to bacterial stimulation but does significantly impact internal circuitry that influences the DC immune response to both gram-negative and gram-positive cell wall components.

Impact of ZIP8 on bacterial stimulation and Zn homeostasis in DCs

To examine the impact of ZIP8 and Zn homeostasis on DC function *in vitro*, Zn transporter expression and Zn content was measured in stimulated BMDCs. Bacterial stimulation induced *Zip8* mRNA expression in WT BMDCs, which was significantly higher than baseline and *Zip8*-KO stimulated counterparts (LPS – $p < 0.001$, LTA – $p < 0.05$; Figure 6A). Despite induction of *Zip8* expression, intracellular Zn content decreased in both groups following LPS and LTA stimulation. *Zip8*-KO DCs had significantly lower available Zn ($p < 0.05$) as measured by the mean fluorescent intensity with ZinPyr-1 staining (Figure 6B).

The observed decrease in available Zn, despite the increase in *Zip8* mRNA in the WT BMDCs, suggested that expression of other Zn transporters may be altered in stimulated BMDCs. Indeed, investigation of other select Zn transporters, namely ZIP-6, −10 and −14, revealed further changes in expression patterns with a modest decrease in the expression of *Zip* 6 and *Zip*10 and an increase in expression of *Zip*14 relative to *Zip*8 (Figure

6C). Collectively, these observations indicate that alteration of intracellular Zn content is consequent to altered expression of multiple Zn transporters, not excluding ZnTs, and that DCs are programmed to reduce Zn content in response to bacteria.

To further elucidate the impact of Zn homeostasis on DC responses after bacterial stimulation, BMDCs were incubated with TPA, a Zn-specific chelator, or supplemented with $ZnSO_4$ and then stimulated overnight with LPS. BMDCs treated with TPA had a net decrease in available Zn content which was further potentiated by LPS stimulation. Comparison of baseline and treated samples revealed that WT BMDCs had significantly lower Zn content after TPA incubation and LPS stimulation ($p = 0.01$) whereas *Zip8*-KO BMDCs exhibited a marginal reduction in available Zn. Conversely, BMDCs treated with $ZnSO_4$ showed a marginal increase in Zn content, which was decreased after LPS stimulation in both groups (Figure 6D).

Alteration of intracellular Zn content corresponded with changes in BMDC cytokine profiles within both groups. Reduction in intracellular Zn following chelation with TPA resulted in increased production of TNF-α in both groups ($p < 0.001$; Figure 6E) and IL-10, but only in WT cells ($p = 0.001$; data not shown). There were however no differences observed in the production of IL-6 and IL-12/23p40 following Zn chelation and LPS stimulation (data not shown). Supplementation with $ZnSO_4$ had little to no effect on cytokine production between the groups, except for TNF-α production, which was significantly decreased in both groups when compared to the TPA and LPS stimulated samples (Figure 6E). Collectively, these results suggest that Zn homeostasis, specifically decreased Zn levels, contributes to differences observed in the immune response of *Zip8*-KO BMDCs following bacterial exposure.

Zip8 loss alters gene expression in DCs after bacterial stimulation.

The absence of phenotypic differences between WT and *Zip8*-KO BMDCs, despite the differences seen in early cytokine production after bacterial stimulation, suggested that there may be alteration in intracellular programs that are associated with immune activation. Analysis of over 700 genes using nCounter® myeloid innate immune gene profiling showed that at baseline there were only 14 genes that were significantly different between the WT and *Zip8*-KO cells (Figure 7A). Further comparison of baseline to bacterial stimulated samples identified 158 genes (WT unstimulated vs bacterial stimulated) and 243 genes (*Zip8*-KO unstimulated vs bacterial stimulated) that were significantly different between the groups (Figure 7A). Comparison of fold change in gene expression between WT and *Zip8*-KO LPS stimulated BMDCs revealed 16 genes that were differentially expressed ($p < 0.05$), with 7 of these genes highly relevant to DC function, namely, antigen presentation, chemokine/cytokine signaling and lymphocyte activation (Figure 7B). Using Ingenuity Pathway Analysis, the DC maturation pathway was identified as the one of top regulatory biological pathway, involving 6 upregulated genes (predominantly involved in the assembly of the MHC-II molecule) from the list of differentially expressed genes in *Zip8*-KO stimulated samples (Figure 7B-C).

Given that tightly regulated gene networks are dedicated to performing specific functions in cellular transcriptomes, upstream regulator analysis (URA) was performed to identify

transcription factors and key genes controlling gene networks between treatment groups. URA predicted that the *NFκB, PI3K*, and *ESR2* transcription factors were significantly upregulated in stimulated *Zip8*-KO BMDCs ($p < 0.01$; z score > 2.0) and may play a central role in controlling expression of gene networks (Figure 7D). Further network analysis found that FGF2 and IFNB1 (cytokines); CCL26 and CCL6 (chemokines); and GLYRP1, HLA-DMB, CD74 and IL-10RA were integral to the NFκB gene network in stimulated *Zip8*-KO BMDCs compared WT BMDCs (Figure 7E). These results show that upregulation of DC maturation pathways and activation of NFκB-mediated signaling, through transcription factors controlling specific sets for chemokines/cytokines, could account for differences observed between LPS stimulated BMDCs from both groups and more so in *Zip8*-KO cultures.

Increased activation of NFκB signaling pathway in Zip8KO BMDCs after LPS stimulation

To determine whether the NFκB signaling pathway, as predicted by IPA analysis, accounted for the differences observed in DC-mediated responses between the groups, we first examined NFκB-related molecules by phospho-Western blotting. LPS, as predicted, increased phosphorylation of IKβα in both groups, but more so in *Zip8*-KO BMDCs at 10, 15 and 30 minutes after stimulation. This response was attenuated in both groups after incubation with BAY 11-7082, an IKK inhibitor (Supplemental Figure 3A). Similar results were observed with nuclear translocation of NFκB 15 minutes post LPS stimulation. *Zip8*-KO BMDCs also exhibited significantly higher NFκB translocation when compared to the WT BMDCs after LPS stimulation, which was diminished in both groups following incubation with BAY 11-7082 (Figure 8A). Similarly, inhibition of NFκB signaling resulted in a significant decrease in production of IL-12/23p40, IL-6, and TNF-α in both groups following LPS stimulation (Figure 8B-E). As observed previously, cytokine production was more pronounced in *Zip8*-KO BMDCs. The blunted cytokine response in both groups persisted up to 24 hours after the stimulus was removed (Supplemental Figure 3C-E). Interestingly, there were no differences observed in the extent of phosphorylation of other signaling molecules associated with production of these cytokines including ERK1/2 and p38 (Supplemental Figure 3B). These results demonstrate that the altered DC response consequent to ZIP8 loss and changes in Zn homeostasis is heavily influenced through augmentation of NFκB signaling.

Loss of ZIP8 alters the Th2/Th17 balance post pneumococcal infection.

Preliminary data from NanoString and IPA analyses predicted that ZIP8 loss is associated with changes in the expression of genes associated with antigen presentation and T-cell activation. Given that DCs play a pivotal role in bridging the gap between innate and adaptive immunity, and that NFκB signaling plays a role in T-cell activation by DCs (42), DCs and T-cells from the mediastinal lymph nodes of WT and *Zip8*-KO mice were examined following *S. pneumoniae* infection. As previously described, mice were infected with 4 x 10^8 CFUs of *S. pneumoniae*, and tissues harvested 72 hours post infection. After gating out doublets, debris, and dead cells, DCs were characterized based on expression of CD11c, MHC-II, CD24 and further divided into 2 subsets based on expression of CD8α (CD8α$^+$ DCs and CD8α$^-$ DCs). T-cells were characterized as either CD4$^+$ T-cells (CD45$^+$CD3$^+$CD4$^+$) or CD8$^+$ T-cells (CD45$^+$CD3$^+$CD8$^+$; Figure 9A). Flow cytometric

analysis of LN cells revealed no differences in total numbers of DC subsets ($CD8\alpha^+$ and $CD8\alpha^-$) or $CD4^+$ T-cells between the groups 72 hours post infection (Figure 9B). However, when whole LN cultures (a mix of DCs and T-cells) isolated from infected animals of both groups were restimulated *in vitro*, stark changes in T-helper cell cytokine profiles were observed. Analysis of the $CD4^+$ T-cell population by flow cytometry revealed a significant decrease in the production of IL-17 from the *Zip8*-KO cultures. Interestingly, this was associated with an increase in the production of IL-4, with no differences observed in the production of IFN-γ and IL-2 between the groups (Figure 9C). Similar results were observed in *Zip8*-KO co-cultures stimulated for 48 hours (Figure 9D). Collectively, results demonstrate that ZIP8 loss distorts Th2/Th17 balance in a manner that is detrimental to the host.

Discussion

In this study, we investigated the role of ZIP8 in the myeloid-mediated immune response to pneumococcal pneumonia. Strikingly, we observed that ZIP8 loss was associated with overall worse outcomes in infected mice resulting in intensification of the inflammatory response, more collateral tissue damage and cell death, and increased mortality. Alteration of the immune response began early after infection and intensified over a period of days. Strikingly, mortality in *Zip8*-KO mice occurred between 72-96 hours post infection. During the first 72 hours post infection, an increase in the numbers of alveolar macrophages and DCs in the lungs of *Zip8*-KO animals occurred. AMs have well established roles in the host defense against *S. pneumoniae* and subsequent resolution of the inflammatory response (27-30). Interestingly, an increase in numbers of AMs was associated with increased bacterial burdens in the spleens of *Zip8*-KO mice indicating that *S. pneumoniae* more readily extravasated out of lung into the systemic circulation resulting in deposition in other tissues. Our previous studies have shown that after bacterial challenge, ZIP8 is significantly upregulated in monocytes and macrophages. This is associated with increased intracellular zinc in these cells; a response that is significantly diminished with siRNA knockdown of ZIP8 (19, 20). Others have shown that the level of intracellular zinc influences the phagocytic capacity of macrophages. In human subjects, zinc deficiency in AMs (caused by alcohol abuse) was shown to impair immune function due to decreased phagocytosis and bacterial clearance (43). More recently, ZIP7 knockdown in THP-1 cells was associated with decreased intracellular Zn and impaired phagocytosis efficiency (44).

Though impaired macrophage phagocytosis is likely a cause of increased bacterial dissemination, aberrant increase in lung DC presence has also been shown to exacerbate the immune response and facilitate extrapulmonary dissemination of bacteria during pneumococcal infection (33, 34). Consistent with this, we observed an increase in the $CD11b^+$ subset of lung DCs in *Zip8*-KO mice following *S. pneumoniae* infection. $CD11b^+$ DCs, both conventional (cDCs) and monocyte-derived (moDCs), have been shown to be induced after allergen exposure (45), viral (46) and fungal infection (47), and were found to be the major subset of DCs that transport *Mycobacterium tuberculosis (M. tb)* to the mediastinal lymph following infection (48). Through the process of antigen presentation following infection, DCs have also been shown to act as an “Achilles heel” or “Trojan horse” of the immune system, inadvertently serving as a vehicle for systemic dissemination

of pathogens that migrate from the periphery to secondary lymphoid organs (49-52). Whether this response is exacerbated due to ZIP8 loss requires further study.

It is also important to recognize that neutrophils may also contribute to increased bacterial dissemination observed in the *Zip8*-KO animals following pneumococcal infection. Although we did not observe significant differences in PMN counts between treatment groups, Zn signals have been shown to play an integral role in ROS-dependent signal transduction leading to neutrophil extracellular traps (NET) formation and subsequent bacterial killing (53). Therefore, further studies are warranted to determine whether phagocytosis and/or NET formation is impaired due to ZIP8 loss. Nevertheless, the increased presence of macrophages and DCs observed in *Zip8*-KO mice occurred in tandem with more inflammation and cell death. This suggests that worse outcomes following pneumococcal pneumonia in the setting of ZIP8 loss is likely a combination of aberrant immune cell function, mediated in part by these two dominant myeloid cell populations, as well as increased collateral tissue damage caused by an exaggerated immune response.

We provide novel evidence that ZIP8 is significantly induced in DCs by bacteria, a response unique among other Zn transporters (19, 21). To our knowledge, there has been only one other study that examined the impact of Zn homeostasis on DC function. Kitamura and colleagues revealed that activation of the TLR4 pathway overall decreased DC cytosolic Zn content which was essential for MHC-II vesicle trafficking and antigen presentation (54). This phenomenon required down-modulation of ZIP6 expression. Consistent with this, we observed a modest reduction in *Zip*6 gene expression in both groups, though not significantly different between the groups. Collectively, the changes in Zn transporter expression resulted in a reduction of available Zn levels, and more so in *Zip8*-KO BMDCs, leading to profound changes in cytokine production in response to bacterial stimulation. These results are in line with previous work in which *Zip*8 knockdown resulted in a reduction of cytosolic Zn in macrophages (19). However, in contrast, further modulation of Zn content did not significantly alter cytokine secretion. This suggests that regulation of DC Zn homeostasis is more sophisticated than just a “wholesale” reduction in cellular Zn content. Given that ZIP8 is also a transporter of other divalent ions including manganese and iron (55-58), it is plausible that some of the ZIP8-mediated changes observed in DCs are not exclusively attributed to alteration of Zn transport. Further studies are warranted to determine the potential contribution of other divalent metal cations, as well as changes in other Zn transporters, to account for the observed alterations following loss of ZIP8 in DCs.

Notwithstanding, we believe that our data suggest that changes in ZIP8 expression leads to Zn redistribution within macrophages, as previously reported (19), as well as DCs at the onset of infection resulting in modulation of molecular signaling pathways that balance the host immune response. Perhaps most striking, LPS stimulated *Zip8*-KO DCs exhibited significant alteration in immune related gene expression profiles that collectively (using Ingenuity Pathway Analysis) predicted alteration in pathways associated with DC maturation and MHC-II antigen presentation. Notably, the genes with the greatest fold increase in the *Zip8*-KO cells (CD74 and H2-Ab1) play a role in the assembly and transport of the MHC-II molecule. Further studies are warranted to determine whether antigen presentation by MHC-II is altered in *Zip8*-KO DCs, since cell surface expression, as

characterized by flow cytometry, was similar between the stimulated groups. The predicted alterations in maturation/antigen presentation in *Zip8*-KO DCs was also associated with a concomitant significant increase in NFκB signaling when compared to WT DCs. NFκB is induced by many activators of DC maturation and has a well-established role in DC function (42, 59-61). Our group has shown that ZIP8 is a negative and essential regulator of NFκB signaling and that it tempers activation in a Zn dependent manner. Studies using monocytes, macrophages, and human lung epithelial cells found that *Zip*8 transcription is directly regulated by NFκB and suppression of *Zip*8 resulted in increased proinflammatory mediators and increased phosphorylation of p65 and IkBα (20). Consistent with these results, we observed a significant increase in NFκB nuclear translocation and consequent cytokine production after LPS stimulation which was significantly ablated by inhibition of NFκB signaling. These findings are significant in the context of DC function given that NFκB is required for DC development, survival, activation and T-cell priming (42, 61, 62). Previous studies have shown that MAPKs, specifically p38 and ERK1/2, play a role in DC cytokine production after bacterial stimulation, however, the extent of ERK and p38 phosphorylation was no different between stimulated WT and KO BMDC cultures. Taken together, this demonstrates that ZIP8 loss in DCs results in increased NFκB activation, similar to what is seen in macrophages, which is a major contributor to aberrant immune function.

Given the vital role that DCs play in bacterial recognition and initiation of the adaptive immune response, we wanted to begin to understand whether ZIP8, or lack thereof, may have a broader impact beyond front-line host defense. In accordance with this, we observed that $CD4^+$ T-cells from the lymph nodes of *Zip8*-KO infected animals were impaired in their ability to produce IL-17. Over the last two decades, a protective role of IL-17 producing $CD4^+$ Th17 cells in the host immune response against pneumococcal infection has emerged. It has been shown that local production of IL-17 plays a significant role in mounting an effective host defense against bacteria by promoting neutrophil and macrophage recruitment, thus enhancing pneumococcal clearance by phagocytes (63, 64). IL-17A has also been shown to stimulate epithelial cells to trigger anti-microbial responses against intracellular bacteria and increased mortality was observed in mice with a deficiency in the IL-17A receptor post infection with *S. pneumoniae* TIGR-4 strain (65). Decreased levels of IL-17A were also found to be associated with increased risk of bacteremia in a *Klebsiella pneumoniae* model (66). In the context of our findings, increased IL-4 production from $CD4^+$ T-cells isolated from the LNs of *Zip8*-KO mice may also contribute further to inhibition of a protective Th17/IL-17 response, which we believe is detrimental to the host. Consistent with this, increased production of IL-4 is associated with systemic bacterial infection and increased mortality following pneumococcal infection (67, 68), with increased bacterial clearance and survival in IL-4 deficient mice following bacterial pneumonia (69). We postulate that the diminished IL-17 response has broader implications in the context of memory responses and long-term protection against pneumococcal infections. Consistent with this, a recent study demonstrated that protection against different *S. pneumoniae* serotypes was mediated primarily by Th17 cells and not antibodies. Immune mice were shown to mount an even stronger IL-17A response compared to initial infection. In addition,

the localized T-helper cell lung response consisted mainly of IL-17A producing $CD4^+$ T-cells, with only a small proportion of IFN-γ producing $CD4^+$ T-cells (70).

Although macrophages are recognized as APCs, DCs are considered more so as professional APCs, that capture antigens in the periphery, migrate to the draining LNs, and then present antigens to naïve T-cells, thus bridging the gap between innate and adaptive immunity. Based on our findings, we contend that T-cell priming in the lung draining mediastinal lymph nodes of *S. pneumoniae* infected mice is mediated primarily by DCs, and that loss of ZIP8 contributes to an impaired T-helper cell response. Given that appropriate T-cell priming is fundamental to activation of the adaptive immune response, future studies are warranted to further elucidate the mechanisms by which ZIP8 mediates T-cell priming/activation, specifically Th17 activation, in the host response against pneumococcal pneumonia. Notwithstanding, these results highlight a complex and vital role for ZIP8-mediated Zn homeostasis relative to cell-to-cell communication.

Zn is required for proper immune function and dietary-induced deficiency is associated with increased susceptibility to pneumococcal infection (12, 13). For example, to combat invading pathogens, the host upregulates the acquisition of critical nutrients (zinc, iron, etc.); a defense known as “nutritional immunity”. While this is classically associated with the restriction of iron, the availability of other transition metals, including manganese and Zn, are also highly regulated by the host. To acquire sufficient Zn, most bacteria possess homologs of Znu/Adc, an ATP-binding cassette (ABC) permease system capable of directly importing labile zinc with nanomolar affinity. These systems are important for the virulence of numerous pathogens, including *Streptococcus pneumoniae* (71-73). We postulate that ZIP8 is upregulated at the onset of bacterial infection resulting in redistribution of Zn within host immune cells. This provides a competitive advantage to the host through immune cell recruitment to contain infection. In the absence of ZIP8 and therefore Zn, this response is substantially augmented, ultimately resulting in acute and possibly long-term outcomes following pneumococcal pneumonia. This is supported by a recent GWAS study in humans that identified a polymorphic variant of *Zip*8 was significantly associated with increased susceptibility to *Staphylococcus aureus* infection (24). This is further supported by a recent study where dietary Zn deficiency enhanced susceptibility to pneumococcal infection in mice caused by alteration of phagocytic function resulting in bacterial dissemination (74). A common genetic variant in ZIP8 (rs13107325; A391T) ranks in the top 10 of pleiotropic single nucleotide polymorphisms (SNP) identified in genome-wide association studies, and *in silico* modeling predicts rs13107325 to be in the top 1.4% of deleterious substitutions in the human genome (75). Given the relatively high frequency of its occurrence and recent studies demonstrating that this ZIP8 variant is commonly associated as a driver of inflammation-based disease (76), we believe our findings to be clinically relevant. Also, given the relatively high occurrence of dietary Zn deficiency in populations that are most susceptible to pneumococcal pneumonia, further studies are warranted to determine whether patients that harbor the A391T allele and whom have poor dietary Zn intake, are even more prone to infection and worse outcomes and whether either or both can be countered with aggressive Zn supplementation strategies.

Taken together, this investigation highlights a previously unidentified link between Zn homoeostasis, myeloid immune cell function, and the host response against pneumococcus in the lung. Our novel findings substantiate that a decrease in available Zn is required for proper DC function but that there also exists an essential ZIP8-dependent, Zn-mediated balance between cellular activation machinery and adaptive immune priming. This further underscore the complexity of essential divalent metal trafficking, not limited to Zn, as a vital component of immune regulation in the battle between host and pathogen. It also warrants future studies that evaluate the impact of both environment (dietary nutrient intake) and genetic composition (for example, Zn regulatory factors) in tandem in the context of host susceptibility to and recovery from infection with commonly occurring pathogens.

Supplementary Material

Refer to Web version on PubMed Central for supplementary material.

Acknowledgment and Support

The UNMC Flow Cytometry Research Facility is administrated through the Office of the Vice Chancellor for Research and supported by state funds from the Nebraska Research Initiative (NRI) and The Fred and Pamela Buffett Cancer Center's National Cancer Institute Cancer Support Grant. Major instrumentation has been provided by the Office of the Vice Chancellor for Research, The University of Nebraska Foundation, the Nebraska Banker's Fund, and by the NIH-NCRR Shared Instrument Program. The authors wish to thank members of the Tissue Sciences Facility at the Department of Pathology and Microbiology Department (University of Nebraska Medical Center) for assistance with lung tissue processing, sectioning, H&E staining, and assistance with digital microscopy images prepared for the manuscript.

This work was supported by the National Institutes of Health [HL118268 (DLK)]. TAW is the recipient of a Research Career Scientist Award (IK6 BX003781) from the Department of Veterans Affairs.

References

1. File TM Jr, Low DE, Eckburg PB, Talbot GH, Friedland HD, Lee J, Llorens L, Critchley I, and Thye D. 2010. Integrated analysis of FOCUS 1 and FOCUS 2: randomized, doubled-blinded, multicenter phase 3 trials of the efficacy and safety of ceftaroline fosamil versus ceftriaxone in patients with community-acquired pneumonia. Clin. Infect. Dis 51: 1395–1405. [PubMed: 21067350]
2. Musher DM, Roig IL, Cazares G, Stager CE, Logan N, and Safar H. 2013. Can an etiologic agent be identified in adults who are hospitalized for community-acquired pneumonia: results of a one-year study. J. Infect 67: 11–18. [PubMed: 23523447]
3. Restrepo MI, Mortensen EM, Velez JA, Frei C, and Anzueto A. 2008. A comparative study of community-acquired pneumonia patients admitted to the ward and the ICU. Chest 133: 610–617. [PubMed: 17989157]
4. Sherwin RL, Gray S, Alexander R, McGovern PC, Graepel J, Pride MW, Purdy J, Paradiso P, and File TM Jr. 2013. Distribution of 13-valent pneumococcal conjugate vaccine Streptococcus pneumoniae serotypes in US adults aged ≥50 years with community-acquired pneumonia. J. Infect. Dis 208: 1813–1820. [PubMed: 24092845]
5. Gonçalves MT, Mitchell TJ, and Lord JM. 2016. Immune ageing and susceptibility to Streptococcus pneumoniae. Biogerontology 17: 449–465. [PubMed: 26472172]
6. Rink L and Kirchner H. 2000. Zinc-altered immune function and cytokine production. J. Nutr 130: 1407S–11S. [PubMed: 10801952]
7. Ibs KH and Rink L. 2003. Zinc-altered immune function. J. Nutr 133: 1452S–6S. [PubMed: 12730441]
8. Fraker PJ, King LE, Laakko T, and Vollmer TL. 2000. The dynamic link between the integrity of the immune system and zinc status. J. Nutr 130: 1399S–406S. [PubMed: 10801951]

9. Fraker PJ and King LE. 2004. Reprogramming of the immune system during zinc deficiency. Annu. Rev. Nutr 24: 277–298. [PubMed: 15189122]
10. Wessells KR and Brown KH. 2012. Estimating the global prevalence of zinc deficiency: results based on zinc availability in national food supplies and the prevalence of stunting. PLoS One 7: e50568. [PubMed: 23209782]
11. Fischer Walker C and Black RE. 2004. Zinc and the risk for infectious disease. Annu. Rev. Nutr 24: 255–275. [PubMed: 15189121]
12. Mocchegiani E, Giacconi R, Muzzioli M, and Cipriano C. 2000. Zinc, infections and immunosenescence. Mech. Ageing Dev 121: 21–35. [PubMed: 11164457]
13. Barnett JB, Hamer DH, and Meydani SN. 2010. Low zinc status: a new risk factor for pneumonia in the elderly? Nutr. Rev 68: 30–37. [PubMed: 20041998]
14. Girodon F, Galan P, Monget AL, Boutron-Ruault MC, Brunet-Lecomte P, Preziosi P, Arnaud J, Manuguerra JC, and Herchberg S. 1999. Impact of trace elements and vitamin supplementation on immunity and infections in institutionalized elderly patients: a randomized controlled trial. MIN. VIT. AOX. geriatric network. Arch. Intern. Med 159: 748–754. [PubMed: 10218756]
15. Girodon F, Lombard M, Galan P, Brunet-Lecomte P, Monget AL, Arnaud J, Preziosi P, and Hercberg S. 1997. Effect of micronutrient supplementation on infection in institutionalized elderly subjects: a controlled trial. Ann. Nutr. Metab 41: 98–107. [PubMed: 9267584]
16. Prasad AS, Beck FW, Bao B, Fitzgerald JT, Snell DC, Steinberg JD, and Cardozo LJ. 2007. Zinc supplementation decreases incidence of infections in the elderly: effect of zinc on generation of cytokines and oxidative stress. Am. J. Clin. Nutr 85: 837–844. [PubMed: 17344507]
17. Bafaro E, Liu Y, Xu Y, and Dempski RE. 2017. The emerging role of zinc transporters in cellular homeostasis and cancer. Signal. Transduct Target Ther 2: 17029. [PubMed: 29218234]
18. Hojyo S and Fukada T. 2016. Zinc transporters and signaling in physiology and pathogenesis. Arch. Biochem. Biophys 611: 43–50. [PubMed: 27394923]
19. Pyle CJ, Akhter S, Bao S, Dodd CE, Schlesinger LS, and Knoell DL. 2017. Zinc Modulates Endotoxin-Induced Human Macrophage Inflammation through ZIP8 Induction and C/EBPβ Inhibition. PLoS One 12: e0169531. [PubMed: 28056086]
20. Liu MJ, Bao S, Gálvez-Peralta M, Pyle CJ, Rudawsky AC, Pavlovicz RE, Killilea DW, Li C, Nebert DW, Wewers MD, and Knoell DL. 2013. ZIP8 regulates host defense through zinc-mediated inhibition of NF-κB. Cell. Rep 3: 386–400. [PubMed: 23403290]
21. Pyle CJ, Azad AK, Papp AC, Sadee W, Knoell DL, and Schlesinger LS. 2017. Elemental Ingredients in the Macrophage Cocktail: Role of ZIP8 in Host Response to Mycobacterium tuberculosis. Int. J. Mol. Sci 18: 2375. doi: 10.3390/ijms18112375. [PubMed: 29120360]
22. Costas J 2018. The highly pleiotropic gene SLC39A8 as an opportunity to gain insight into the molecular pathogenesis of schizophrenia. Am. J. Med. Genet. B. Neuropsychiatr. Genet 177: 274–283. [PubMed: 28557351]
23. Pickrell JK, Berisa T, Liu JZ, Ségurel L, Tung JY, and Hinds DA. 2016. Detection and interpretation of shared genetic influences on 42 human traits. Nat. Genet 48: 709–717. [PubMed: 27182965]
24. Ye Z, Vasco DA, Carter TC, Brilliant MH, Schrodi SJ, and Shukla SK. 2014. Genome wide association study of SNP-, gene-, and pathway-based approaches to identify genes influencing susceptibility to Staphylococcus aureus infections. Front. Genet 5: 125. [PubMed: 24847357]
25. Guilliams M, Lambrecht BN, and Hammad H. 2013. Division of labor between lung dendritic cells and macrophages in the defense against pulmonary infections. Mucosal Immunol. 6: 464–473. [PubMed: 23549447]
26. Kopf M, Schneider C, and Nobs SP. 2015. The development and function of lung-resident macrophages and dendritic cells. Nat. Immunol 16: 36–44. [PubMed: 25521683]
27. Aberdein JD, Cole J, Bewley MA, Marriott HM, and Dockrell DH. 2013. Alveolar macrophages in pulmonary host defence the unrecognized role of apoptosis as a mechanism of intracellular bacterial killing. Clin. Exp. Immunol 174: 193–202. [PubMed: 23841514]
28. Dockrell DH, Marriott HM, Prince LR, Ridger VC, Ince PG, Hellewell PG, and Whyte MK. 2003. Alveolar macrophage apoptosis contributes to pneumococcal clearance in a resolving model of pulmonary infection. J. Immunol 171: 5380–5388. [PubMed: 14607941]

29. Guillon A, Arafa EI, Barker KA, Belkina AC, Martin I, Shenoy AT, Wooten AK, Lyon De Ana C, Dai A, Labadorf A, Hernandez Escalante J, Dooms H, Blasco H, Traber KE, Jones MR, Quinton LJ, and Mizgerd JP. 2020. Pneumonia recovery reprograms the alveolar macrophage pool. JCI Insight 5: e133042. doi: 10.1172/jci.insight.133042. [PubMed: 31990682]
30. Knapp S, Leemans JC, Florquin S, Branger J, Maris NA, Pater J, van Rooijen N, and van der Poll T. 2003. Alveolar macrophages have a protective antiinflammatory role during murine pneumococcal pneumonia. Am. J. Respir. Crit. Care Med 167: 171–179. [PubMed: 12406830]
31. Hammad H and Lambrecht BN. 2007. Lung dendritic cell migration. Adv. Immunol 93: 265–278. [PubMed: 17383544]
32. Worbs T, Hammerschmidt SI, and Forster R. 2017. Dendritic cell migration in health and disease. Nat. Rev. Immunol 17: 30–48. [PubMed: 27890914]
33. Winter C, Taut K, Länger F, Mack M, Briles DE, Paton JC, Maus R, Srivastava M, Welte T, and Maus UA. 2007. FMS-like tyrosine kinase 3 ligand aggravates the lung inflammatory response to Streptococcus pneumoniae infection in mice: role of dendritic cells. J. Immunol 179: 3099–3108. [PubMed: 17709524]
34. Rosendahl A, Bergmann S, Hammerschmidt S, Goldmann O, and Medina E. 2013. Lung dendritic cells facilitate extrapulmonary bacterial dissemination during pneumococcal pneumonia. Front. Cell. Infect. Microbiol 3: 21. [PubMed: 23802100]
35. Knoell DL, Smith D, Bao S, Sapkota M, Wyatt TA, Zweier JL, Flury J, Borchers MT, and Knutson M. 2020. Imbalance in zinc homeostasis enhances lung Tissue Loss following cigarette smoke exposure. J. Trace Elem. Med. Biol 60: 126483. [PubMed: 32155573]
36. Trouplin V, Boucherit N, Gorvel L, Conti F, Mottola G, and Ghigo E. 2013. Bone marrow-derived macrophage production. J. Vis. Exp (81):e50966. doi: e50966. [PubMed: 24300014]
37. Inaba K, Inaba M, Romani N, Aya H, Deguchi M, Ikehara S, Muramatsu S, and Steinman RM. 1992. Generation of large numbers of dendritic cells from mouse bone marrow cultures supplemented with granulocyte/macrophage colony-stimulating factor. J. Exp. Med 176: 1693–1702. [PubMed: 1460426]
38. Livak KJ and Schmittgen TD. 2001. Analysis of relative gene expression data using real-time quantitative PCR and the 2(-Delta Delta C(T)) Method. Methods 25: 402–408. [PubMed: 11846609]
39. Dyavar SR, Mykris TM, Winchester LC, Scarsi KK, Fletcher CV, and Podany AT. 2020. Hepatocytic transcriptional signatures predict comparative drug interaction potential of rifamycin antibiotics. Sci. Rep 10: 12565-020-69228-z.
40. Dyavar SR, Potts LF, Beck G, Dyavar Shetty BL, Lawson B, Podany AT, Fletcher CV, Amara RR, and Papa SM. 2020. Transcriptomic approach predicts a major role for transforming growth factor beta type 1 pathway in L-Dopa-induced dyskinesia in parkinsonian rats. Genes Brain Behav. 19: e12690. [PubMed: 32741046]
41. Dyavar Shetty R, Velu V, Titanji K, Bosinger SE, Freeman GJ, Silvestri G, and Amara RR. 2012. PD-1 blockade during chronic SIV infection reduces hyperimmune activation and microbial translocation in rhesus macaques. J. Clin. Invest 122: 1712–1716. [PubMed: 22523065]
42. O'Sullivan BJ and Thomas R. 2002. CD40 ligation conditions dendritic cell antigen-presenting function through sustained activation of NF-kappaB. J. Immunol 168: 5491–5498. [PubMed: 12023343]
43. Mehta AJ, Yeligar SM, Elon L, Brown LA, and Guidot DM. 2013. Alcoholism causes alveolar macrophage zinc deficiency and immune dysfunction. Am. J. Respir. Crit. Care Med 188: 716–723. [PubMed: 23805851]
44. Xie W, Xue Q, Niu L, and Wong KW. 2020. Zinc transporter SLC39A7 relieves zinc deficiency to suppress alternative macrophage activation and impairment of phagocytosis. PLoS One 15: e0235776. [PubMed: 32645059]
45. Plantinga M, Guilliams M, Vanheerswynghels M, Deswarte K, Branco-Madeira F, Toussaint W, Vanhoutte L, Neyt K, Killeen N, Malissen B, Hammad H, and Lambrecht BN. 2013. Conventional and monocyte-derived CD11b(+) dendritic cells initiate and maintain T helper 2 cell-mediated immunity to house dust mite allergen. Immunity 38: 322–335. [PubMed: 23352232]

46. Lukens MV, Kruijsen D, Coenjaerts FE, Kimpen JL, and van Bleek GM. 2009. Respiratory syncytial virus-induced activation and migration of respiratory dendritic cells and subsequent antigen presentation in the lung-draining lymph node. J. Virol 83: 7235–7243. [PubMed: 19420085]
47. Osterholzer JJ, Chen GH, Olszewski MA, Curtis JL, Huffnagle GB, and Toews GB. 2009. Accumulation of CD11b+ lung dendritic cells in response to fungal infection results from the CCR2-mediated recruitment and differentiation of Ly-6Chigh monocytes. J. Immunol 183: 8044–8053. [PubMed: 19933856]
48. Wolf AJ, Linas B, Trevejo-Nuñez GJ, Kincaid E, Tamura T, Takatsu K, and Ernst JD. 2007. Mycobacterium tuberculosis infects dendritic cells with high frequency and impairs their function in vivo. J. Immunol 179: 2509–2519. [PubMed: 17675513]
49. Bierly AL, Shufesky WJ, Sukhumavasi W, Morelli AE, and Denkers EY. 2008. Dendritic cells expressing plasmacytoid marker PDCA-1 are Trojan horses during Toxoplasma gondii infection. J. Immunol 181: 8485–8491. [PubMed: 19050266]
50. Izquierdo-Useros N, Naranjo-Gómez M, Erkizia I, Puertas MC, Borràs FE, Blanco J, and Martinez-Picado J. 2010. HIV and mature dendritic cells: Trojan exosomes riding the Trojan horse? PLoS Pathog. 6: e1000740. [PubMed: 20360840]
51. Schönrich G and Raftery MJ. 2015. Dendritic cells as Achilles' heel and Trojan horse during varicella zoster virus infection. Front. Microbiol 6: 417. [PubMed: 26005438]
52. Williams NL, Morris JL, Rush CM, and Ketheesan N. 2014. Migration of dendritic cells facilitates systemic dissemination of Burkholderia pseudomallei. Infect. Immun 82: 4233–4240. [PubMed: 25069976]
53. Hasan R, Rink L, and Haase H. 2013. Zinc signals in neutrophil granulocytes are required for the formation of neutrophil extracellular traps. Innate Immun. 19: 253–264. [PubMed: 23008348]
54. Kitamura H, Morikawa H, Kamon H, Iguchi M, Hojyo S, Fukada T, Yamashita S, Kaisho T, Akira S, Murakami M, and Hirano T. 2006. Toll-like receptor-mediated regulation of zinc homeostasis influences dendritic cell function. Nat. Immunol 7: 971–977. [PubMed: 16892068]
55. Choi EK, Nguyen TT, Gupta N, Iwase S, and Seo YA. 2018. Functional analysis of SLC39A8 mutations and their implications for manganese deficiency and mitochondrial disorders. Sci. Rep 8: 3163-018-21464-0.
56. Scheiber IF, Alarcon NO, and Zhao N. 2019. Manganese Uptake by A549 Cells is Mediated by Both ZIP8 and ZIP14. Nutrients 11: 1473. doi: 10.3390/nu11071473. [PubMed: 31261654]
57. van Raaij SEG, Srai SKS, Swinkels DW, and van Swelm RPL. 2019. Iron uptake by ZIP8 and ZIP14 in human proximal tubular epithelial cells. Biometals 32: 211–226. [PubMed: 30806852]
58. Wang CY, Jenkitkasemwong S, Duarte S, Sparkman BK, Shawki A, Mackenzie B, and Knutson MD. 2012. ZIP8 is an iron and zinc transporter whose cell-surface expression is up-regulated by cellular iron loading. J. Biol. Chem 287: 34032–34043. [PubMed: 22898811]
59. Dev A, Iyer S, Razani B, and Cheng G. 2011. NF-κB and innate immunity. Curr. Top. Microbiol. Immunol 349: 115–143. [PubMed: 20848362]
60. Rescigno M, Martino M, Sutherland CL, Gold MR, and Ricciardi-Castagnoli P. 1998. Dendritic cell survival and maturation are regulated by different signaling pathways. J. Exp. Med 188: 2175–2180. [PubMed: 9841930]
61. Ouaaz F, Arron J, Zheng Y, Choi Y, and Beg AA. 2002. Dendritic cell development and survival require distinct NF-kappaB subunits. Immunity 16: 257–270. [PubMed: 11869686]
62. van de Laar L, van den Bosch A, van der Kooij SW, Janssen HL, Coffer PJ, van Kooten C, and Woltman AM. 2010. A nonredundant role for canonical NF-κB in human myeloid dendritic cell development and function. J. Immunol 185: 7252–7261. [PubMed: 21076069]
63. Marqués JM, Rial A, Muñoz N, Pellay FX, Van Maele L, Léger H, Camou T, Sirard JC, Benecke A, and Chabalgoity JA. 2012. Protection against Streptococcus pneumoniae serotype 1 acute infection shows a signature of Th17- and IFN-γ-mediated immunity. Immunobiology 217: 420–429. [PubMed: 22204818]
64. Wang W, Zhou A, Zhang X, Xiang Y, Huang Y, Wang L, Zhang S, Liu Y, Yin Y, and He Y. 2014. Interleukin 17A promotes pneumococcal clearance by recruiting neutrophils and inducing

apoptosis through a p38 mitogen-activated protein kinase-dependent mechanism in acute otitis media. Infect. Immun 82: 2368–2377. [PubMed: 24664502]

65. Ritchie ND, Ritchie R, Bayes HK, Mitchell TJ, and Evans TJ. 2018. IL-17 can be protective or deleterious in murine pneumococcal pneumonia. PLoS Pathog. 14: e1007099. [PubMed: 29813133]
66. Ye P, Garvey PB, Zhang P, Nelson S, Bagby G, Summer WR, Schwarzenberger P, Shellito JE, and Kolls JK. 2001. Interleukin-17 and lung host defense against Klebsiella pneumoniae infection. Am. J. Respir. Cell Mol. Biol 25: 335–340. [PubMed: 11588011]
67. Mizrachi-Nebenzahl Y, Lifshitz S, Teitelbaum R, Novick S, Levi A, Benharroch D, Ling E, and Dagan R. 2003. Differential activation of the immune system by virulent Streptococcus pneumoniae strains determines recovery or death of the host. Clin. Exp. Immunol 134: 23–31. [PubMed: 12974750]
68. Woytschak J, Keller N, Krieg C, Impellizzieri D, Thompson RW, Wynn TA, Zinkernagel AS, and Boyman O. 2016. Type 2 Interleukin-4 Receptor Signaling in Neutrophils Antagonizes Their Expansion and Migration during Infection and Inflammation. Immunity 45: 172–184. [PubMed: 27438770]
69. Song Z, Zhang J, Zhang X, Li D, Wang H, Xu X, Xu W, Yin Y, and Cao J. 2015. Interleukin 4 Deficiency Reverses Development of Secondary Pseudomonas aeruginosa Pneumonia During Sepsis-Associated Immunosuppression. J. Infect. Dis 211: 1616–1627. [PubMed: 25489003]
70. Wang Y, Jiang B, Guo Y, Li W, Tian Y, Sonnenberg GF, Weiser JN, Ni X, and Shen H. 2017. Cross-protective mucosal immunity mediated by memory Th17 cells against Streptococcus pneumoniae lung infection. Mucosal Immunol. 10: 250–259. [PubMed: 27118490]
71. Bayle L, Chimalapati S, Schoehn G, Brown J, Vernet T, and Durmort C. 2011. Zinc uptake by Streptococcus pneumoniae depends on both AdcA and AdcAII and is essential for normal bacterial morphology and virulence. Mol. Microbiol 82: 904–916. [PubMed: 22023106]
72. Brown LR, Caulkins RC, Schartel TE, Rosch JW, Honsa ES, Schultz-Cherry S, Meliopoulos VA, Cherry S, and Thornton JA. 2017. Increased Zinc Availability Enhances Initial Aggregation and Biofilm Formation of Streptococcus pneumoniae. Front. Cell. Infect. Microbiol 7: 233. [PubMed: 28638805]
73. Makthal N, Do H, Wendel BM, Olsen RJ, Helmann JD, Musser JM, and Kumaraswami M. 2020. Group A Streptococcus AdcR Regulon Participates in Bacterial Defense against Host-Mediated Zinc Sequestration and Contributes to Virulence. Infect. Immun 88: e00097–20. doi: 10.1128/IAI.00097-20. Print 2020 Jul 21. [PubMed: 32393509]
74. Eijkelkamp BA, Morey JR, Neville SL, Tan A, Pederick VG, Cole N, Singh PP, Ong CY, Gonzalez de Vega R, Clases D, Cunningham BA, Hughes CE, Comerford I, Brazel EB, Whittall JJ, Plumptre CD, McColl SR, Paton JC, McEwan AG, Doble PA, and McDevitt CA. 2019. Dietary zinc and the control of Streptococcus pneumoniae infection. PLoS Pathog. 15: e1007957. [PubMed: 31437249]
75. Zhang R, Witkowska K, Afonso Guerra-Assunção J, Ren M, Ng FL, Mauro C, Tucker AT, Caulfield MJ, and Ye S. 2016. A blood pressure-associated variant of the SLC39A8 gene influences cellular cadmium accumulation and toxicity. Hum. Mol. Genet 25: 4117–4126. [PubMed: 27466201]
76. Sunuwar L, Frkatovic A, Sharapov S, Wang Q, Neu H, Wu X, Haritunians T, Wan F, Michel SLJ, Wu S, McGovern D, Lauc G, Donowitz M, Sears CL, and Melia JM. 2020. Pleiotropic ZIP8 A391T implicates abnormal manganese homeostasis in complex human disease. JCI Insight

Key Points

- ZIP8 is upregulated in macrophages and DCs after bacterial stimulation.
- ZIP8 loss augments lung inflammation, bacterial dissemination, and mortality.
- ZIP8 loss increases NFκB signaling and alters T-cell priming.

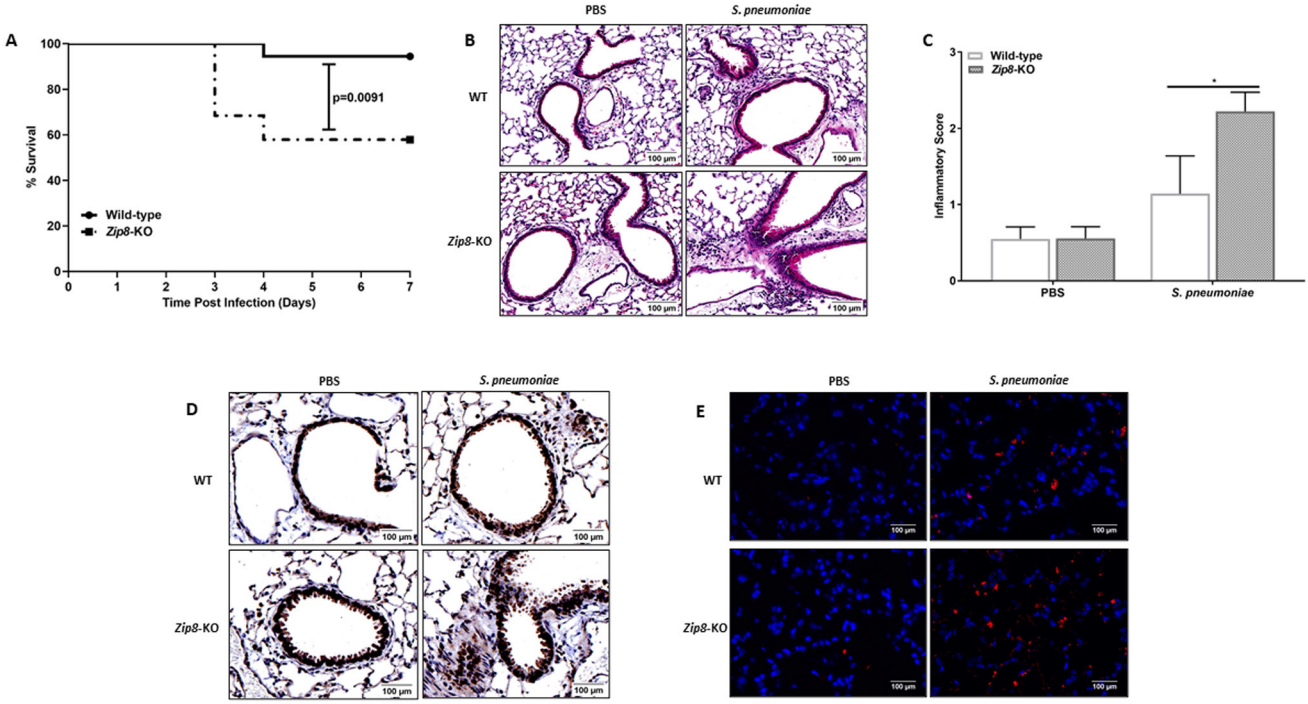

Figure 1.

Loss of ZIP8 in myeloid cells is associated with increased mortality and lung injury following pneumococcal infection. (A) WT and *Zip8*-KO mice were infected with on average 4 x 10^8 CFUs of *S. pneumoniae* and survival was monitored out to 7 days. Next, WT and *Zip8*-KO mice were infected with 4 x 10^8 CFUs *S. pneumoniae* and lung samples were harvested at 72 hours post infection. Lung tissue was examined for (B) H&E-stained histopathology, (C) corresponding inflammatory scores, (D) caspase-3 staining and (E) TUNEL staining. Caspase-3 and TUNEL staining are representative of multiple images from multiple animals. (Magnification: x 20 – H&E, x 40 – caspase-3 and TUNEL staining; scale bars = 100 μm). Data are presented as the mean ± SEM and represent at least two independent studies. (n=18-19 mice per group (A), n=7-8 mice per group (B-D); *$p \leq 0.05$)

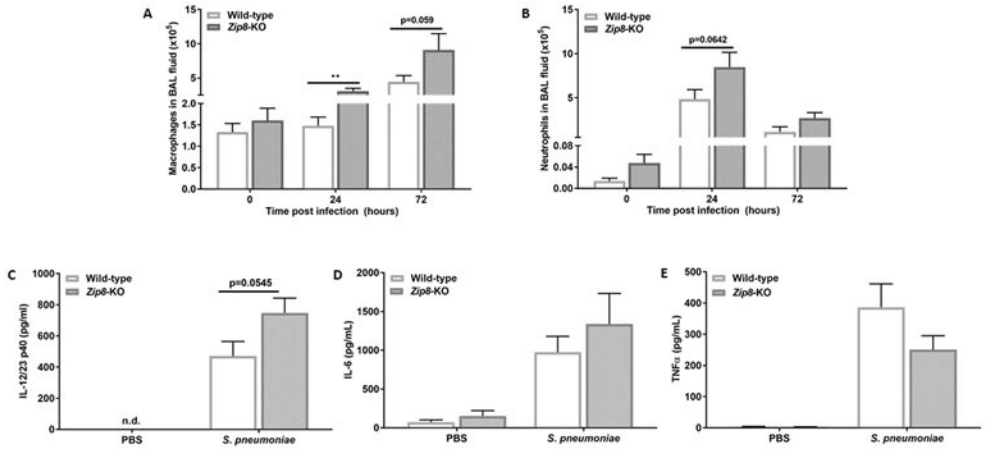

Figure 2.

Analysis of broncho-alveolar lavage fluid for cellularity, cytokine, and chemokine content following *S. pneumoniae* instillation. WT and *Zip8*-KO mice were administered 4 x 10^8 CFU *S. pneumoniae* intranasally and euthanized 24 or 72 hours later. Lungs were lavaged with PBS, cells collected, counted, immobilized on glass slides, and stained for morphological characterization for (A) total macrophage and (B) neutrophil cell counts. (C-E) Cell-free BAL fluid was also analyzed by ELISA (C) IL-12/23p40 (D) IL-6 and (E) TNF-α 24 hours post infection. Data are presented as the mean ± SEM and represent at least two to three independent studies. (n=18-19 mice per group (24 hours) and 7-8 mice per group (72 hours); **p < 0.01).

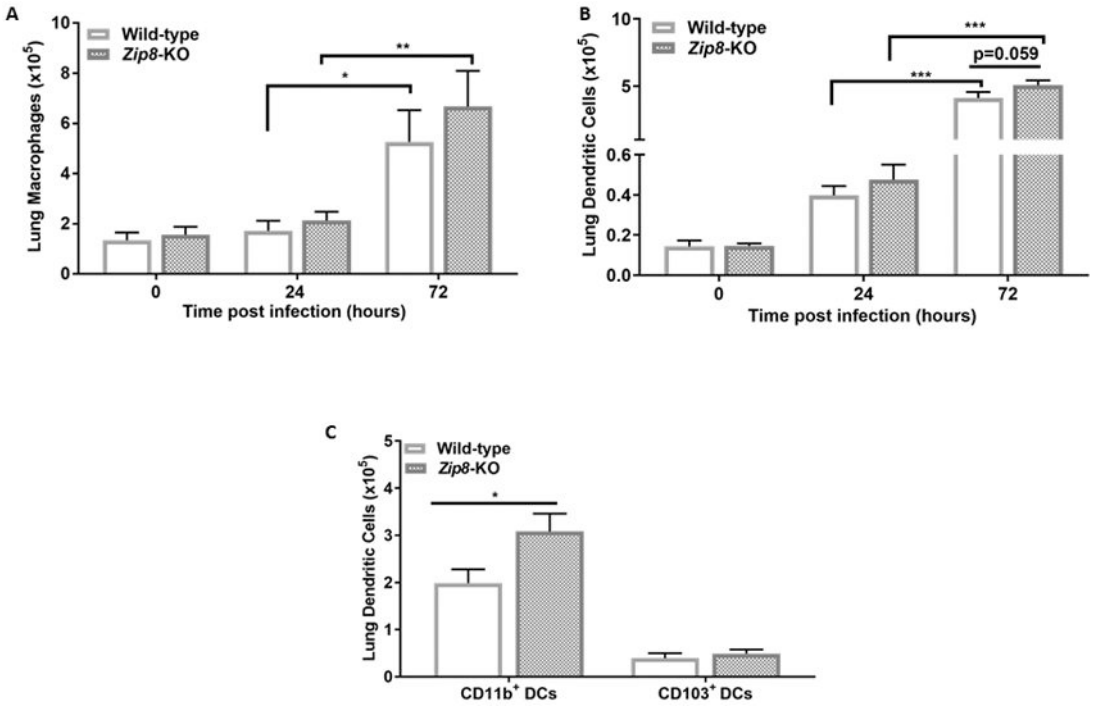

Figure 3.

Phenotypic characterization of alveolar macrophages and lung DCs 24 and 72 hours post pneumococcal infection. Lung homogenates from uninfected and infected WT and *Zip8*-KO mice were phenotyped by flow cytometry analysis. After gating out debris and doublets, live $CD45^+$ leukocytes were selected. Cells were characterized as AMs, based on expression of CD11c, Siglec F and CD64 ($CD45^+CD11c^+$Siglec F^+CD64^+), or DCs, based on expression of classic DC markers ($CD45^+CD24^+CD64^-CD11c^+$MHC-$II^+$). DC subsets were then identified based on expression of CD11b or CD103. (A) Quantification of total numbers of macrophages, (B) lung DCs and (C) DC subsets in lung homogenates of *S. pneumoniae* infected WT and *Zip8*-KO animals. Data are presented as the mean ± SEM and represent two to three independent studies. (n= 8-15 mice per group; *$p < 0.05$, **$p < 0.01$, ***$p < 0.001$).

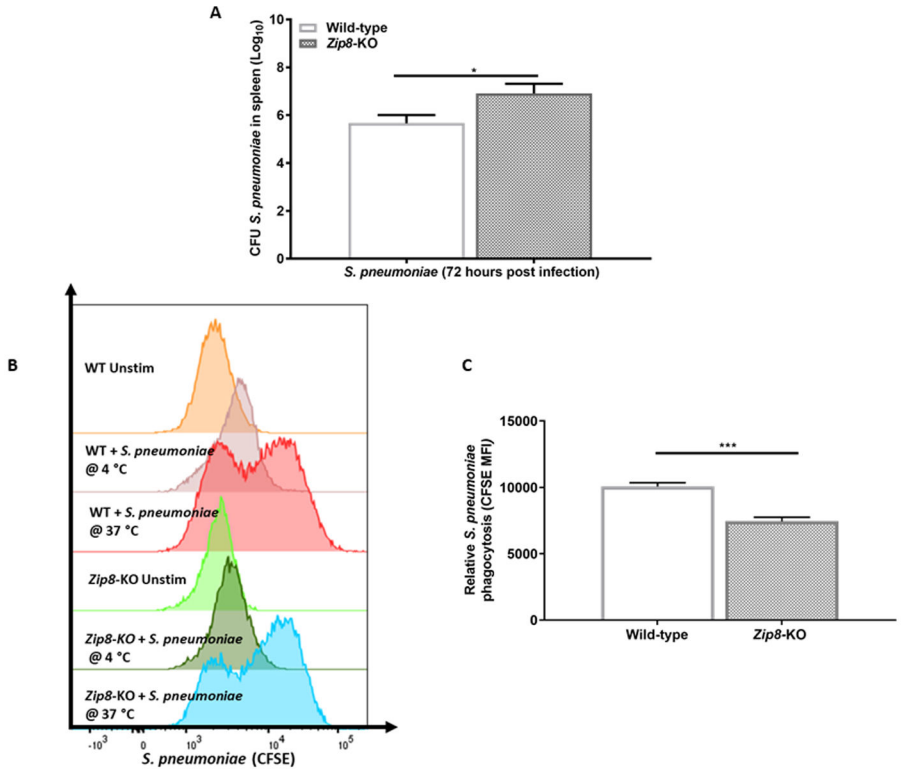

Figure 4.

Loss of ZIP8 is associated with increased bacterial dissemination and impaired macrophage phagocytosis. (A) WT and *Zip8*-KO animals were infected with *S. pneumoniae* (4 x 10^8 CFUs) and bacterial load in spleen homogenates assessed 72 hours post infection. BMDMs were then generated from uninfected WT and *Zip8*-KO mice, incubated with CFSE labelled *S. pneumoniae* for 1 hour, and bacterial uptake determined by flow cytometry. Cells were gated as macrophages based on expression of cell surface markers ($CD11b^+CD24^-CD64^+$) and bacterial uptake quantified based on CFSE expression. (B) Representative flow histograms of noninfected and infected cultures at 4 °C and 37 °C. (C) Quantification of bacterial uptake as a measure of the median fluorescent intensity of CFSE, after subtracting the MFI of the control sample at 4 °C from that of the test sample at 37 °C (MFI CFSE $_{\text{sample}}$ = MFI CFSE $_{\text{sample @37 °C}}$ − MFI CFSE $_{\text{sample @4°C}}$). Data are presented as the mean ± SEM and represent at least two independent studies. (n =10-13 mice per group (*in vivo*); n = 6-8 samples per group (*in vitro*); *p < 0.05, ***p < 0.001).

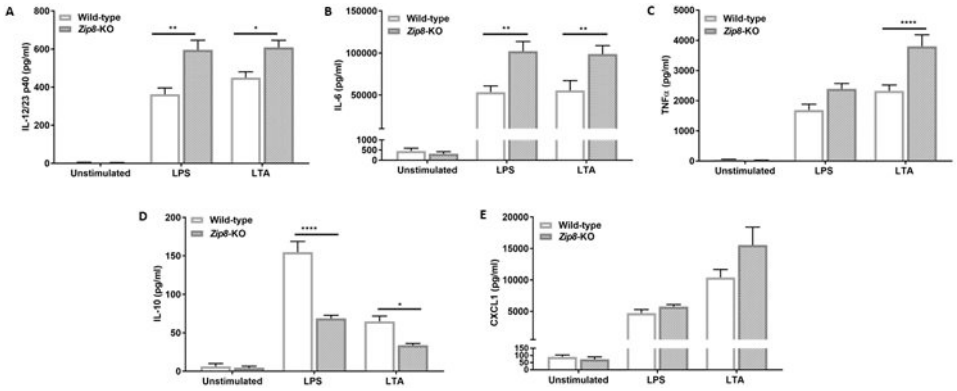

Figure 5.

Cytokine production from BMDCs following stimulation with gram negative and gram-positive bacterial cell wall products *in vitro*. BMDCs from WT and *Zip8*-KO mice were stimulated with either LPS (1 μg/ml) or LTA (10 μg/ml) for 6 hours. (A-E) Cytokine production of IL-12/23p40, IL-6, TNF-α, IL-10 and CXCL-1 from LPS/LTA stimulated or unstimulated BMDCs was compared and measured by ELISA. Data are presented as the mean ± SEM and represent at least four independent studies. (n= 16 samples per group; *$p < 0.05$, **$p < 0.01$, ****$p < 0.0001$).

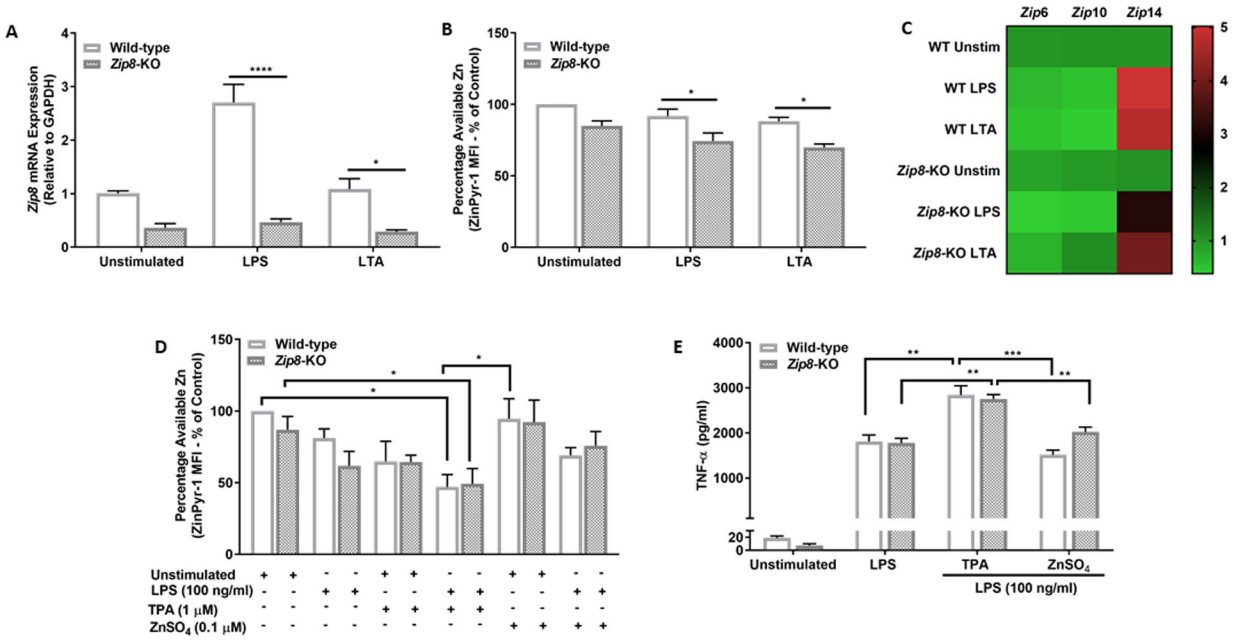

Figure 6.

Effects of bacterial stimulation on Zn homeostasis in BMDCs. WT and *Zip8*-KO BMDCs were stimulated with LPS (1 μg/ml) or LTA (10 μg/ml) for 6 hours and cells were then harvested for analysis of select Zn transporter gene expression and cytosolic Zn content. (A) *Zip8* mRNA expression in WT and *Zip8*-KO BMDCs after stimulation with LPS or LTA. (B) Semi-quantitative cytosolic Zn levels at baseline and in stimulated BMDCs as measured by ZinPyr-1 staining and FACS. Zn levels were quantified as median fluorescent intensity (MFI). (C) Heat map of gene expression of *Zip6*, *Zip10* and *Zip14* in LPS- and LTA-pulsed BMDCs from both groups. (D-E) BMDCs from WT and *Zip8*-KO mice were then incubated with either 1 μM TPA or 0.1 μM $ZnSO_4$ for 30 minutes then stimulated with LPS (100 ng/ml) for 24 hours. Semi-quantitative cytosolic zinc expression (D) and TNF-α production (E) following Zn manipulation and LPS stimulation in BMDCs isolated from both groups. Data are presented as the mean ± SEM and represent at least three independent studies. (n= 9 samples per group; *p < 0.05, **p < 0.01, ***p < 0.001).

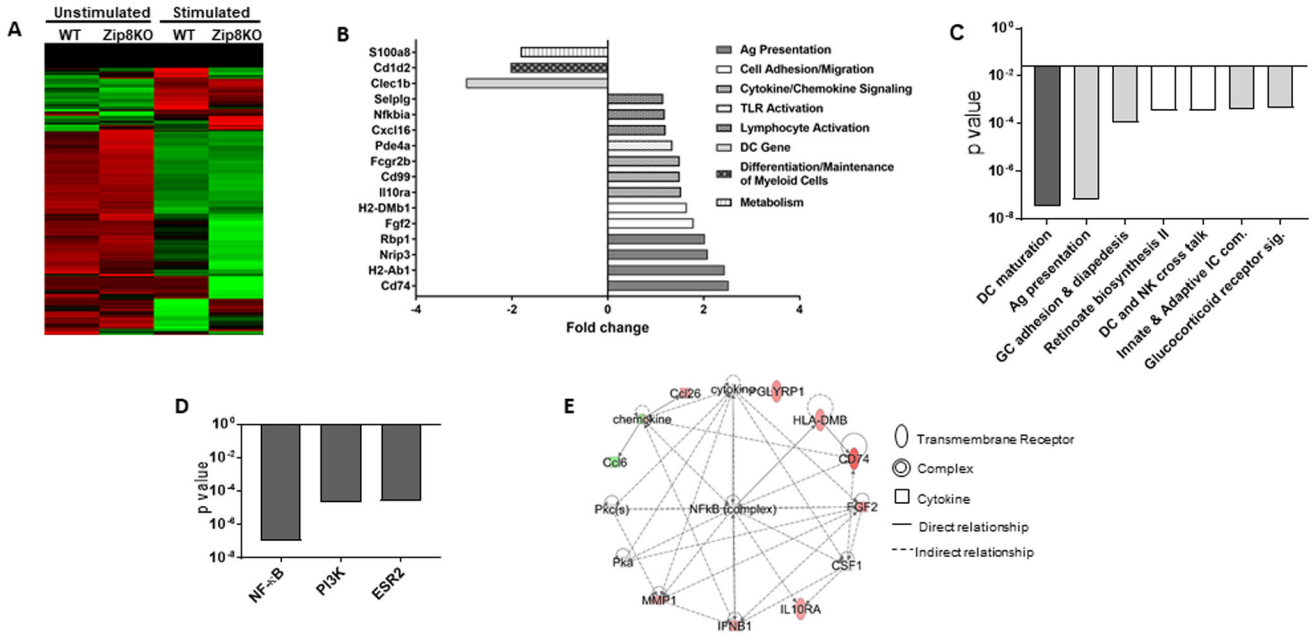

Figure 7.

Loss of Zip8 alters the immune gene expression profile in DCs after bacterial stimulation. BMDCs were stimulated with LPS, harvested and then RNA was isolated for NanoString and IPA analyses. (A) Heat map of gene expression between the WT and Zip8-KO unstimulated versus stimulated BMDCs. Data was generated using unsupervised clustering and normalized to a scale that gives equal variance to all the differentially expressed genes. Green indicates high and red indicates low expression. (B) Specific pathways significantly ($p < 0.01$) regulated in LPS stimulated *Zip8*-KO BMDCs in comparison to WT BMDCs. Dark grey bars indicate a positive Z score; light grey bars indicate no activity pattern and empty bars had a '0' Z score. (C) Fold change of genes (and associated pathways) in stimulated DCs from both groups (positive values indicate the genes that were upregulated in the *Zip8*-KO cultures compared to WT cultures (D) Upregulation of transcription factors in stimulated *Zip8*-KO BMDCs ($p < 0.0001$ p value and >2.0 Z score). Dark grey bars indicate a positive Z score. (E) NF-κB transcriptional network was identified as a leading pathway in stimulated BMDCs from *Zip8*-KO BMDCs compared to WT BMDCs. Genes that are positively (red) or negatively (green) regulated either directly or indirectly under the influence of NFκB in *Zip8*-KO BMDCs are shown. (Data was generated from 3 samples per group from 3 independent studies).

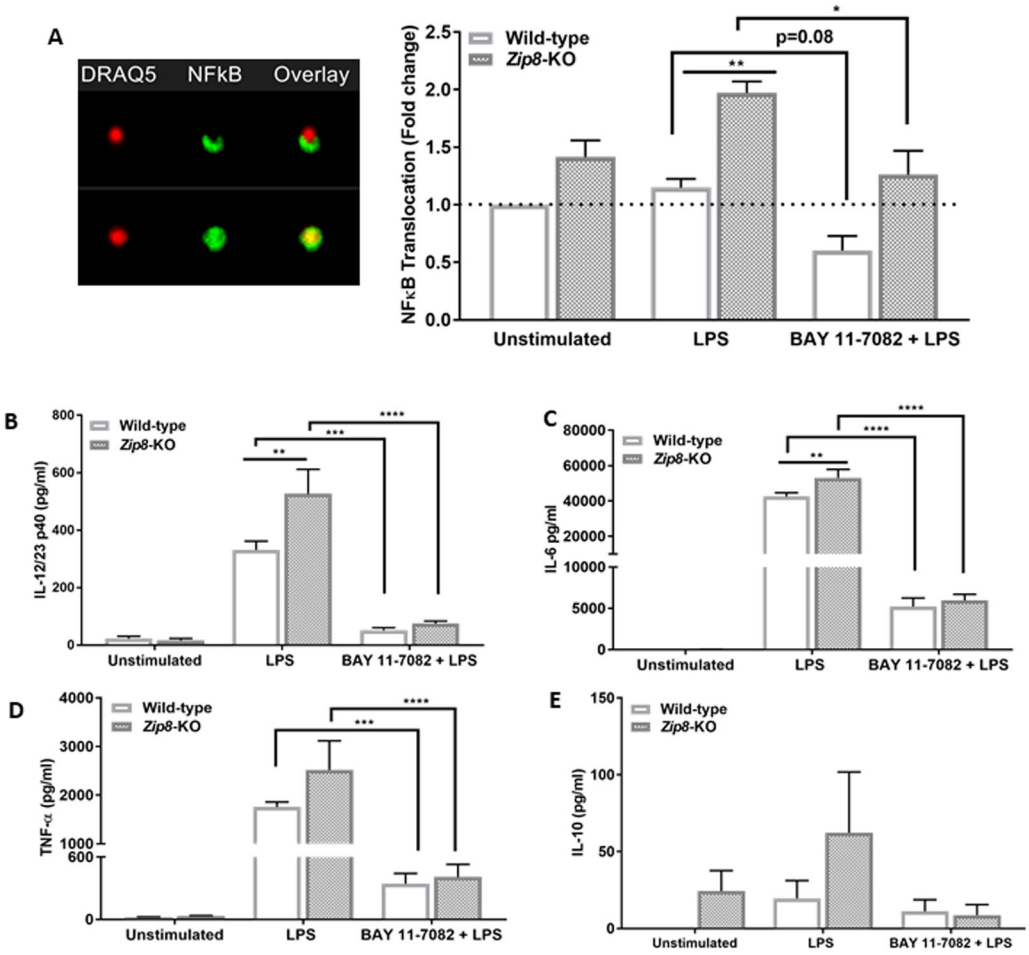

Figure 8.

NFκB signaling and corresponding cytokine production is greater in *Zip8*-KO BMDCs after LPS stimulation. BMDCs from WT and *Zip8*-KO animals were stimulated with LPS (1 μg/ml) only, or also with an IKK inhibitor (BAY 11-7082; 10 μM) for 1 hour, followed by LPS stimulation. At the indicated time points cells were harvested, fixed, permeabilized, stained and analyzed by flow cytometry, and supernatants were collected for analysis of cytokine production. (A) Fold change in NFκB nuclear translocation following BAY 11-7082 inhibition for 1 hour and/or LPS stimulation (1 μg/ml) for 15 minutes in WT and *Zip8-KO* BMDCs. (B-D) Cytokine profiles from WT and *Zip8-KO* BMDC cultures following ± BAY 11-7082 and then LPS stimulation for 6 hours. Data are presented as the mean ± SEM and represent two independent studies. (n=6-12 samples per group; *p ≤0.05, **p < 0.01, ***p < 0.001, ****p < 0.0001).

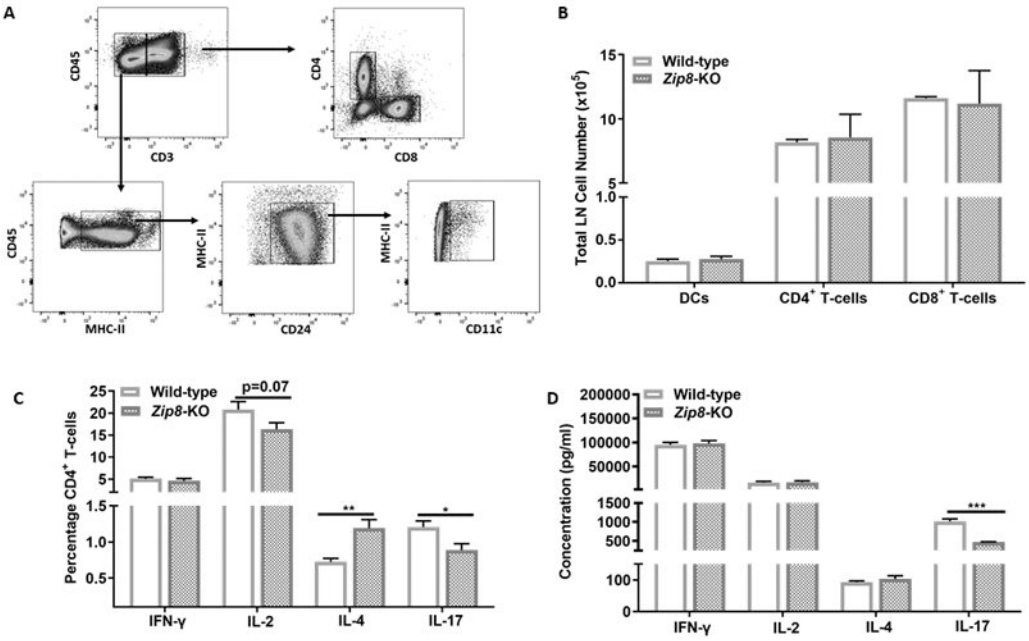

Figure 9.

Zip8 loss alters communication between DCs and T-cells. WT and *Zip8*-KO mice were infected with 4 x 10^8 CFU *S. pneumoniae* and mediastinal lymph nodes harvested 72 hours post infection. In some experiments, cells were restimulated *in vitro* with PMA (10 ng/ml) and ionomycin (250 ng/ml) for the indicated time points with or without Brefeldin A (5 μg/ml). (A) Gating strategy used to phenotype DCs and T-cells and (B) quantification of total DCs ($CD8\alpha^+$ and $CD8\alpha^-$ subsets), $CD4^+$ T-cells and $CD8^+$ T-cells from LN homogenates of infected mice. (C) T-helper cell cytokine production from $CD4^+$ T-cell subsets (with Brefeldin A for 4 hours) and (D) whole LN mixed cell cultures (without Brefeldin A for 48 hours) from infected WT and *Zip8*-KO animals. Data are presented as the mean ± SEM and represent two independent studies. (n=14 animals per group; *p < 0.05, **p < 0.01 ***p < 0.001).